Vacuum–UV fluorescence spectroscopy of CCl4, SiCl4 and GeCl4 in the range 9–25eV

Biehl, H.; Baumgärtel, H.; Jochims, H.w.; Boyle, Kenneth; Seccombe, Dominic; Smith, DM; Tuckett, Richard

DOI:
10.1016/S0368-2048(98)00261-8

ELSEVIER

Journal of Electron Spectroscopy and Related Phenomena 97 (1998) 89–113

JOURNAL OF ELECTRON SPECTROSCOPY and Related Phenomena

Vacuum–UV fluorescence spectroscopy of CCl_4, $SiCl_4$ and $GeCl_4$ in the range 9–25 eV ☆

H. Biehl[a], K.J. Boyle[a], D.P. Seccombe[a], D.M. Smith[a,1], R.P. Tuckett[a,*], H. Baumgärtel[b], H.W. Jochims[b]

[a]*School of Chemistry, University of Birmingham, Edgbaston, Birmingham B15 2TT, UK*
[b]*Institut fur Physikalische und Theoretische Chemie, Freie Universitat Berlin, Takustrasse 3, 14195 Berlin, Germany*

Received 5 March; accepted 27 May 1998

Abstract

The vacuum–ultraviolet (UV) and visible spectroscopy of MCl_4 (M = C, Si, Ge) using fluorescence excitation and dispersed emission techniques is reported. Fluorescence excitation spectra have been recorded following photoexcitation with monochromatised synchrotron radiation in the vacuum–UV energy range 9–25 eV with an average resolution of ca. 0.06 eV. All the peaks in the Rydberg spectra that photodissociate to a fluorescing state of a fragment have been assigned. The Rydberg states arise predominantly from electron excitation from one of the Cl $3p\pi$ non-bonding molecular orbitals of MCl_4, and quantum defects for the Rydberg states characteristic of a chlorine atom are obtained. Dispersed emission spectra in the UV/visible region have been recorded with an optical resolution of ca. 4–8 nm at the energies of the peaks in the excitation spectra. Five different decay channels are observed: (a) CCl_2 $\tilde{A}^1B_1$–$\tilde{X}^1A_1$ fluorescence at ca. 420–600 nm from CCl_4 excited in the range 9–12 eV, (b) $SiCl_2$/$GeCl_2$ $\tilde{a}^3B_1$–$\tilde{X}^1A_1$ and $\tilde{A}^1B_1$–$\tilde{X}^1A_1$ fluorescence from $SiCl_4$/$GeCl_4$ excited in the range 9–14 eV, (c) $SiCl_4^+$/$GeCl_4^+$ $\tilde{C}^2T_2$–$\tilde{X}^2T_1$ and $\tilde{C}^2T_2$–$\tilde{A}^2T_2$ fluorescence at ca. 350–700 nm from $SiCl_4$/$GeCl_4$ for photon energies above the adiabatic ionisation energy of the $\tilde{C}^2T_2$ state of $SiCl_4^+$/$GeCl_4^+$ (15.0 and 14.6 eV, respectively), (d) CCl $A^2\Delta$–$X^2\Pi$ fluorescence at ca. 276–280 nm from CCl_4 excited in the range 14–18eV, and (e) Si* and Ge* atomic emission lines at wavelengths below 310 nm from $SiCl_4$/$GeCl_4$ excited in the range 19–25 eV. These assignments are confirmed by action spectra in which the energy of the vacuum–UV radiation is scanned with detection of the fluorescence at a fixed, dispersive wavelength. By using the single-bunch mode of synchrotron radiation, lifetimes of all the emitting states that fall in the range ca. 4–100 ns have been measured. The MCl_2^* products are formed by photodissociation of low-lying Rydberg states of MCl_4; the thresholds for their production therefore relate to energies of Rydberg states of the parent molecule. The CCl*, Si* and Ge* products are formed by sequential, multi-step photodissociation of MCl_2^*; the thresholds for these emissions correspond to the thermodynamic thresholds to form the emitting product with either three (in the case of CCl*) or four (in the case of Si*/Ge*) chlorine atoms.

Keywords: VUV spectrosopy; Synchrotron radiation; Fluorescence excitation; Dispersed emission; Lifetimes; CCl_4, $SiCl_4$, $GeCl_4$

1. Introduction

It is a pleasure to write for this special issue on ''Unstable Molecules, Reaction Intermediates, and Weakly Bound Complexes''. Our interest is in the spectroscopy of small free radicals and molecular

* Corresponding author. Tel.: + 44-121-414-4425; Fax: + 44-121-414-4426; e-mail: r.p.tuckett@bham.ac.uk.

☆ Dedicated to Professor Neville Jonathan to mark his retirement.

[1] Permanent address: Department of Chemistry, University of Exeter, Exeter EX4 4QD, UK.

0368-2048/98/$ - see front matter
PII: S0368-2048(98)00261-8

ions in the gas phase, unstable species which are well known to be important intermediates in many combustion and plasma processes. The two groups comprising the authors of this paper have collaborated recently to study the photodissociation dynamics of both the Rydberg states of small-to-medium (four to six atoms) polyatomic molecules and the valence states of their parent molecular ion. Specifically, our experiments are sensitive to those Rydberg states that photodissociate to an excited state of a fragment free radical that fluoresces, and to valence states of the parent molecular ion that fluoresce. If AB_n represents a general polyatomic molecule, these two processes can be represented as:

$$AB_n + h\nu_1 \rightarrow (AB_n)^* \rightarrow (AB_{n-1})^* + B$$

$$\text{or } (AB_{n-2})^* + 2B$$

$$(AB_{n-1})^* \text{or } (AB_{n-2})^* \rightarrow AB_{n-1} \text{ or } AB_{n-2} + h\nu_2 \quad (1)$$

and

$$AB_n + h\nu_1 \rightarrow (AB_n^+)^* + e^-$$

$$(AB_n^+)^* \rightarrow AB_n^+ + h\nu_2 \quad (2)$$

$h\nu_1$ and $h\nu_2$ represent photons in the vacuum–ultraviolet (VUV, $50 < \lambda_1 < 150$ nm) and ultraviolet/visible ($200 < \lambda_2 < 700$ nm), respectively. Processes (1) and (2) lead to *resonant* and *non-resonant* peaks, respectively, in the VUV fluorescence excitation spectrum of AB_n. Process (1) is termed resonant, because the VUV photon must populate resonantly the Rydberg state of AB_n. Process (2) is termed non-resonant because, as in photoelectron spectroscopy, signal is still observed for photon energies in excess of the threshold to produce $(AB_n^+)^*$ because the electron can remove the excess energy. These two processes therefore lead to different peak shapes in the fluorescence excitation spectrum [1]. These experiments have become possible in the last 10 to 15 years through the availability of *tunable* VUV radiation operating over a wide range of energies in this region of the electromagnetic spectrum from monochromatised synchrotron sources. It has therefore been possible to populate, state-selectively and often at vibrational resolution, Rydberg states and valence molecular ion states of a range of polyatomic molecules in the energy range ca. 8–25 eV.

In a series of papers [2–6] we have reported the observation and analysis of the non-dispersed fluorescence and dispersed emission spectra following VUV excitation of a range of halides of Groups III, IV and V of the Periodic Table. To date, we have performed experiments on BCl_3 [2], BBr_3 [3], CF_3X (X = F, Cl, Br, H) [4], SiF_4 [5] and PF_3 [6]. Many of these compounds are either used widely or are involved indirectly in the radiofrequency (RF) plasma etching of semiconductor devices. The use of VUV photons affords a softer and more controllable method of excitation than low-energy plasma electrons covering the same energy range. Furthermore, photodissociation of the Rydberg states of such molecules can afford a controlled methodology to produce specific excited states of neutral free radicals (e.g., BCl_2, BBr_2, CF_3, CF_2, SiF_3, SiF_2, PF_2, PF). In this paper we report the results of a study of fluorescence processes following VUV photoexcitation of CCl_4, $SiCl_4$ and $GeCl_4$.

Of these three molecules, CCl_4 has been the most extensively studied in the VUV by other groups using a variety of excitation methods. Causley and Russell [7] observed the absorption spectrum down to 115 nm, and assigned the transitions between 115 and 150 nm as excitations of an electron from one of the Cl $3p\pi$ non-bonding molecular orbitals to Rydberg states of CCl_4. (As shown later, we observe many of these transitions in CCl_4 not by direct absorption, but by photodissociation of the same Rydberg states to fluorescing states of fragment radicals.) There have been two previous VUV synchrotron studies that are pertinent to our work. Ibuki et al. [8] recorded both absolute absorption cross-sections and fluorescence excitation spectra for CCl_4 down to 100 nm. From the appearance energy of the emission in this experiment and from the dispersed emission spectra obtained using Ar I resonance (11.6 eV) and H Lyman-α (10.2 eV) irradiation, the fluorescence in the synchrotron experiment was assigned, indirectly, to $CCl_2\,\tilde{A}^1B_1$–$\tilde{X}^1A_1$. Absolute values of the fluorescence cross-sections and quantum yields for $CCl_2\,\tilde{A}$–$\tilde{X}$ emission were measured in a similar experiment by Lee and Suto [9]. Using tunable low-energy (0–100 eV) electron excitation, Tokue et al. [10, 11] have studied the emission from electron impact excitation of CCl_4. $CCl_2\,\tilde{A}$–$\tilde{X}$, $Cl_2\,D'2^3\Pi_g$–$A'2^3\Pi_u$ and $CCl\,A^2\Delta$–$X^2\Pi$ emissions dominate the spectrum, and thresholds for these emissions and

lifetimes of the emitters have been measured. Tiee et al. [12] have studied the fluorescence from CCl_4 following multi-photon ArF (6.4 eV) laser irradiation, and observe the same molecular bands as seen by Tokue et al. The emission from CCl_4 excited by rare gas metastable atoms Ar* ($^3P_2$, 11.5_5 eV) and He* (^3S, 19.8 eV) has been studied by Tsuji et al. [13]. With Ar* excitation, CCl_2 $\tilde{A}$–$\tilde{X}$ dominates the spectrum. With the higher energy of He* excitation, CCl A–X and bands in Cl_2 (especially D'–A') dominate. Finally, we should note that in an earlier study of our group to look for radiative decay from excited valence states of CCl_4^+, no emission could be observed [14]. Specifically, at the energies of the $\tilde{C}^2T_2$ and $\tilde{D}^2A_1$ states of CCl_4^+, no signal could be detected, although these states of CF_4^+ are known to fluoresce strongly [15]. The fluorescence quantum yields of these states of CCl_4^+ must therefore be very low (probably less than ca. 10^{-5}).

$SiCl_4$ has also been studied in absorption down to 115 nm both by Causley and Russell [7] and by Ibuki et al. [16] and, as with CCl_4, transitions assigned to excitation of Cl $3p\pi$ non-bonding electrons to Rydberg states of $SiCl_4$. Absolute absorption cross-sections and photoionisation quantum yields have been measured in the range 50–100 nm by Kameta et al. [17]. In a recent synchrotron study that is particularly pertinent to our work, Ibuki et al. [18] have measured the absolute fluorescence cross-section of $SiCl_4$ down to 40 nm. In the energy range 10–14 eV, resonants peaks (as in process (1)) are observed in the fluorescence excitation spectrum which are assigned to transitions to Rydberg states of $SiCl_4$ which photodissociate to the $\tilde{a}^3B_1$ and $\tilde{A}^1B_1$ states of $SiCl_2$; emission is then observed as the $\tilde{a}^3B_1$–$\tilde{X}^1A_1$ and $\tilde{A}^1B_1$–$\tilde{X}^1A_1$ bands in $SiCl_2$. At energies above 15.0 eV, a non-resonant peak (as in process (2)) is observed in the excitation spectrum where emission is now due to an excited valence state of the parent ion, in this case the $\tilde{C}^2T_2$ state of $SiCl_4^+$ whose adiabatic ionisation energy is 15.0 eV [19]. We also observed emission from the $\tilde{C}^2T_2$ state of $SiCl_4^+$ in one of our earlier synchrotron experiments [14] and measured the lifetime of this state to be 38.4 ns [15], a value since confirmed by threshold photoelectron–fluorescence coincidence spectroscopy [19]. No measurements were made at the time on $SiCl_4$ for photon energies below 15 eV.

$GeCl_4$ has been the least studied molecule by VUV spectroscopies. A low-resolution absorption spectrum has been observed [7], and we observed non-resonant radiative decay from the $\tilde{C}^2T_2$ state of $GeCl_4^+$ and measured the lifetime of this state to be 65 ns [14, 15]. However, as with $SiCl_4$, no measurements were made then at photon energies below the ionisation energy of $GeCl_4$. Very recently, Ibuki and Kamamoto [20] have observed absolute absorption and fluorescence cross-sections for $GeCl_4$ between 6 and 31 eV using synchrotron radiation. Assignments are given for transitions to Rydberg states of $GeCl_4$ below the first ionisation energy which photodissociate, in a similar manner to $SiCl_4$ [18], to the $\tilde{a}^3B_1$ and $\tilde{A}^1B_1$ states of $GeCl_2$.

In all of these fluorescence studies using synchrotron radiation, the nature of the emitting species has been deduced from other experiments. In this paper we report the results of a definitive experiment to observe *directly* the nature of the emitters when CCl_4, $SiCl_4$ and $GeCl_4$ are excited by tunable VUV radiation. The induced fluorescence at defined excitation energies is dispersed through a secondary monochromator. As shown by the groups of Ibuki and Tsuji, such experiments are common using fixed-energy metastable atom and discharge lamp sources, but are rare using dispersed radiation from a second-generation synchrotron source. We believe that our work complements but extends that of Ibuki et al. on these three Group IV chlorides [8, 18, 20], who could only measure dispersed emission spectra at a small number of VUV energies. We are able to make such measurements at *any* VUV energy within the range of the monochromator used to disperse the synchrotron radiation, and therefore measure the thresholds directly for the different fluorescence decay channels. By using the pulsed, single-bunch mode of the synchrotron we are also able to measure radiative lifetimes which can help to identify the emitter.

2. Experimental

Experiments were performed at synchrotron sources at Daresbury, UK and Bessy 1, Germany. Full details are given elsewhere [5, 6, 21]. Non-dispersed, fluorescence excitation spectra were

recorded at Daresbury using a 1 m Seya-Namioka monochromator (range 8–35 eV, best resolution 0.05 nm) attached to the 2 GeV electron storage ring as the primary source of tunable radiation. Two gratings mounted back-to-back served to cover this wide energy range, and all our experiments used the lower-energy grating (range 8–20 eV). Dispersed fluorescence, vacuum–UV action spectra and lifetime measurements were performed at Bessy 1, using a 1.5 m normal-incidence monochromator (range 7–25 eV, optimum resolution 0.03 nm) attached to the 800 MeV electron storage ring to monochromatise the radiation.

At Daresbury, monochromatised synchrotron radiation entered the interaction region through a glass capillary. The differential pumping provided by the capillary ensured that experiments could be performed windowless at wavelengths below the lithium fluoride cutoff of ca. 110 nm. The fluorescence produced from a sodium-salicylate-coated Pyrex window located behind the interaction region monitored the VUV photon flux for normalisation purposes. Second-order radiation has been estimated to contribute less than ca. 15% of the flux only for photon energies below 10 eV with this grating of the Seya [22]. The photon beam crossed an effusive spray of MCl_4 (pressure ca. 10^{-4} torr) which originated from a hypodermic needle. Fluorescence induced at the interaction region was focused through a quartz window by an aluminium-coated spherical concave mirror onto an EMI 9813 QB photomultiplier tube (range ca. 190–650 nm) maintained at 298 K. The tube operated in the photon-counting mode, and optical filters could be inserted in front of it to isolate different emission bands. Fluorescence excitation spectra were recorded at a resolution of 0.4 nm using the multi-bunch mode of the synchrotron. Spectra were normalised to the VUV flux, and the background fluorescence was subtracted.

At Bessy 1, synchrotron radiation passed from the primary monochromator through a large stainless-steel cube (side 12 cm) and through two stages of differential pumping into a small brass cube (side 5 cm) which served as the interaction region. Vertical (10 mm × 3 mm) and horizontal (1 mm × 5 mm) slits served both for differential pumping and for alignment purposes. A removable LiF window could be positioned prior to the exit slit of the primary monochromator. MCl_4 vapour effused into the brass cube. The pressure within the large stainless-stell cube was typically ca. 2×10^{-5} torr, the pressure within the interaction region was higher although it could not be measured directly. The induced fluorescence was dispersed by a 0.2 m focal length monochromator (Jobin Yvon H20UV or H20VIS). This secondary monochromator had no entrance slit, and a fixed exit slit giving a reciprical dispersion of 4 nm mm^{-1}. Fluorescence was detected either by an EMI 9789 QB photomultiplier tube at 298 K or by an enhanced red-sensitive Hamamatsu R6060 tube cooled to 280 K, both used in the photon-counting mode. The EMI tube was used with the H20UV monochromator, giving an effective range of ca. 190–500 nm. In later experiments, the Hamamatsu tube was used with the H20VIS monochromator, giving an effective range of ca. 190–700 nm. In practice, we used the former system to detect most efficiently the UV fluorescence bands ($\lambda_2 <$ ca. 400 nm), the latter to detect most efficiently the visible bands ($\lambda_2 >$ ca. 400 nm) and to make lifetime measurments because of the fast response of the Hamamatsu tube.

In the multi-bunch mode the following three experiments were possible. First, as at Daresbury, fluorescence excitation spectroscopy, in which the secondary monochromator was set to zero order and the primary monochromator was scanned. Second, action spectroscopy, in which the secondary monochromator was set to a specific fluorescence wavelength and the primary monochromator was scanned. Third, dispersed fluorescence spectroscopy, in which the induced fluorescence was dispersed for a fixed VUV photoexcitation energy. Neither the action nor the dispersed spectra were normalised to the sensitivity curves of the primary or secondary monochromators, respectively, and the fluorescence excitation spectra, in practice, were only used to confirm superior spectra obtained at Daresbury. Both monochromators were calibrated using the N_2^+ $B^2\Sigma_u^+$–$X^2\Sigma_g^+(0,0)$ emission band at 391 nm with production threshold of 18.76 eV.

In the single-bunch mode, lifetimes of the emitting states were measured at Bessy in a manner described elsewhere [6]. The VUV excitation energy (E_1) and the emission wavelength (λ_2) were defined. Fluorescence pulses from the Hamamatsu photomultiplier tube (rise time ca. 1.5 ns) were used as the start signal

Table 1
Energetics of dissociation channels of CCl_4 and CCl_4^+

Neutral/parent ion		Dissociation channel	Dissociation energy (eV)	Vertical (adiabatic) IE (eV)[a]
CCl_4^+	$\tilde{D}^2A_1$			19.9 (19.2)[b]
	$\tilde{C}^2T_2$			16.68 (16.34)
		CCl $A^2\Delta$ + 3Cl	14.32	
	$\tilde{B}^2E$			13.37 (ca. 13.1)
	$\tilde{A}^2T_2$			12.51 (12.27)
		CCl $A^2\Delta$ + Cl_2 + Cl	11.84	
CCl_4^+	$\tilde{X}^2T_1$			11.64 (11.47)
		CCl $X^2\Pi$ + 3Cl	9.86	
		CCl $X^2\Pi$ + Cl_2 + Cl	7.38	
		CCl_2 $\tilde{X}^1A_1$ + Cl_2 $D'2^3\Pi_g$	10.53[c]	
		CCl_2 $\tilde{A}^1B_1$ + 2Cl	8.05	
		CCl_2 $\tilde{X}^2A_1$ + 2Cl	5.91	
		CCl_2 $\tilde{A}^1B_1$ + Cl_2	5.57	
		CCl_2 $\tilde{X}^1A_1$ + Cl_2	3.43	
		CCl_3 $\tilde{C}^2A_1'(3s)$[d] + Cl	ca. 7.8	
		CCl_3 $\tilde{X}^2A_1$[e] + Cl	2.94	
CCl_4	$\tilde{X}^1A_1$			0

[a] Bassett and Lloyd [24].
[b] Creasey et al. [25].
[c] Energy of the Cl_2 $D'2^3\Pi_g$ state from Tellinghuisen and Chakraborty [26].
[d] Symmetry of the lowest Rydberg state of CF_3 [27], assuming D_{3h} planar geometry.
[e] Symmetry of the ground electronic state of CF_3 [27], assuming C_{3v} pyramidal geometry.

to a time-to-amplitude converter (Ortec 567). The synchrotron bunch marker (20 ps pulses every 208 ns, the transit time of electrons around the Bessy storage ring) was used as the stop signal. The resulting decay data were collected in real time with a multichannel analyser card (Ortec 916-002) mounted in a personal computer. Some preliminary lifetime data were recorded using the single-bunch mode at Daresbury. However, we have found that the ability of the Bessy apparatus to disperse the fluorescence, and hence define λ_2, makes this a preferable source for such experiments. Under some circumstances, this dispersion can enable the identity and electronic state of the emitting species to be defined [5, 6]. The lifetime data were analysed using a non-linear least-squares program, FLUOR [23], in which the effects of the ''prompt'' instrument function were deconvoluted from each measured decay trace. Data could be fit to single- or double-exponential functions of the form

$$y = A_1 \exp(-t/\tau_1) + A_2 \exp(-t/\tau_2) + B \quad (3)$$

from which lifetimes (τ_1, τ_2), amplitudes (A_1, A_2) and the background (B) could be obtained. The effective range of lifetimes that can be measured by this technique at Bessy spans the range ca. 3–100 ns. Shorter lifetimes become increasingly difficult to deconvolute effectively from the time response of the electronics. Longer lifetimes cannot be measured because of the relatively small time between synchrotron pulses (208 ns), and the associated problems of wraparound. Note that the 4.8 MHz high repetition rate of this pulsed source is both an advantage and disadvantage for such experiments; decays in the range ca. 3–100 ns collect very quickly, but the upper limit of the lifetime that can be measured is relatively short.

3. The energetics and dissociation channels of $MCl_4^{(+)}$ (M = C, Si, Ge)

The electron configuration of the five highest-occupied outer-valence molecular orbitals of MCl_4 is $\ldots(2a_1)^2(2t_2)^6(1e)^4(3t_2)^6(1t_1)^6$. The numbering scheme does not include core orbitals, and can therefore be used for all three of the compounds studied in this work: CCl_4, $SiCl_4$ and $GeCl_4$. These orbitals arise from the overlap of the 16 chlorine atom valence orbitals, Cl 3*s*,3*p*, with the central atom valence

Table 2
Energetics of dissociation channels of $SiCl_4$ and $SiCl_4^+$

Neutral/parent ion		Dissociation channel	Dissociation energy (eV)	Vertical (adiabatic) IE (eV)[a]
		Si* $^1D_2(3p^1 3d^1)$ + 4Cl	22.3_0	
		Si* $^1P_1(3p^1 4p^1)$ + 4Cl	22.2_9	
		Si* $^3D_1(3p^1 3d^1)$ + 4Cl	22.0_4	
		Si* $^1P_1(3p^1 4s^1)$ + 4Cl	21.5_1	
		Si* $^3P_0(3p^1 4s^1)$ + 4Cl	21.3_5[b]	
$SiCl_4^+$	$\tilde{D}^2A_1$			18.1 (18.1)
		Si $^1S_0(3p^2)$ + 4Cl	18.3_4	
		Si $^1D_2(3p^2)$ + 4Cl	17.2_1	
		Si $^3P_0(3p^2)$ + 4Cl	16.4_3	
	$\tilde{C}^2T_2$			15.3 (15.0)
	$\tilde{B}^2E$			13.5 (13.2)
	$\tilde{A}^2T_2$			13.0 (12.6)
$SiCl_4^+$	$\tilde{X}^2T_1$			12.1 (11.8)
		SiCl + 3Cl	12.6_0	
		SiCl + Cl_2 + Cl	10.1_2	
		$SiCl_2$ $\tilde{A}^1B_1$ + 2Cl	11.3_0	
		$SiCl_2$ $\tilde{a}^3B_1$ + 2Cl	9.9_3	
		$SiCl_2$ $\tilde{A}^1B_1$ + Cl_2	8.8_2[c]	
		$SiCl_2$ $\tilde{X}^1A_1$ + 2Cl	7.5_8	
		$SiCl_2$ $\tilde{a}^3B_1$ + Cl_2	7.4_5[c]	
		$SiCl_2$ $\tilde{X}^1A_1$ + Cl_2	5.1_0	
		$SiCl_3$ + Cl	4.1	
$SiCl_4$	$\tilde{X}^1A_1$			0

[a] Smith et al. [19].
[b] Threshold for fluorescence is 21.8 ± 0.2 eV (Fig. 5(a)).
[c] Energies of the $\tilde{A}^1B_1$ and $\tilde{a}^3B_1$ states of $SiCl_2$ above the $\tilde{X}^1A_1$ ground state from Karolczak and Clouthier [28] and Du et al. [29], respectively.

orbitals, e.g., C 2*s*,2*p*. Adiabatic and vertical ionisation energies (AIE, VIE) are given in Tables 1–3, the data being taken either from He I or threshold photoelectron spectroscopy [19, 24]. The energies of the neutral dissociation channels of CCl_4 and $SiCl_4$ are calculated from 0 K heats of formation given in the Janaf tables [31], with the exception of that of the CCl_3 radical where we use the value established by Hudgens et al. [32]. The data for CCl_4 are probably accurate to the second decimal point in energy units of eV, whereas with that of $SiCl_4$ the second decimal point should probably be treated with caution. Data for the neutral dissociation channels from $GeCl_4$ are not available in the Janaf tables; we use data derived from two relatively old sources [33, 34], and only quote one decimal point in the energies (in eV) of these channels.

Since resonant peaks are observed in the fluorescence excitation spectra of all three molecules at photon energies *below* the AIE of the ground state of the parent ion, fluorescence must be due to one or more neutral fragment(s). In Tables 1–3, therefore, we also show the energies of the low-lying excited valence states of MCl_x ($x = 1$–3). For the trichloride species, the first Rydberg state of CCl_3 has been observed in absorption [35, 36] and higher Rydberg states characterised by resonance-enhanced multiphoton ionisation (REMPI) spectroscopy [37], but no emission spectra from this radical have definitively been observed. Similarly, excited states of $SiCl_3$ and $GeCl_3$ that fluoresce are not known. The first excited state of singlet spin symmetry ($\tilde{A}^1B_1$) of MCl_2 is now well established for all three species [38, 28, 30], although there was some controversy about the origin of the $GeCl_2$ $\tilde{A}$–$\tilde{X}$ transition in the last decade [30, 39]. The analogous triplet states with the same orbital configuration ($\tilde{a}^3B_1$) in $SiCl_2$ and $GeCl_2$ are also now well characterised, the former at vibrational [40, 29], the latter at rotational resolution [30]. The energy of the lowest triplet state of CCl_2, although predicted from ab initio calculations [41], is not

Table 3
Energetics of dissociation channels of $GeCl_4$ and $GeCl_4^+$

Neutral/parent ion		Dissociation channel	Dissociation energy (eV)	Vertical (adiabatic) IE (eV)[a]
		Ge* $^1P_1(4p^15p^1)$ + 4Cl	19.8	
		Ge* $^1P_1(4p^15s^1)$ + 4Cl	19.1[b]	
		Ge* $^3P_1(4p^15s^1)$ + 4Cl	18.8[c]	
$GeCl_4^+$	$\tilde{D}^2A_1$			18.2 (18.2)
	$\tilde{C}^2T_2$			14.9 (14.6)
		Ge $^1S_0(4p^2)$ + 4Cl	16.1	
		Ge $^1D_2(4p^2)$ + 4Cl	15.0	
		Ge $^3P_0(4p^2)$ + 4Cl	14.1	
	$\tilde{B}^2E$			13.1 (12.8)
	$\tilde{A}^2T_2$			12.6, 12.7_5[d] (12.4)
$GeCl_4^+$	$\tilde{X}^2T_1$			12.0, 12.2[d] (11.7)
		GeCl + 3Cl	10.4	
		GeCl + Cl_2 + Cl	7.9	
		$GeCl_2$ $\tilde{A}^1B_1$ + 2Cl	9.8[e]	
		$GeCl_2$ $\tilde{a}^3B_1$ + 2Cl	8.8[e]	
		$GeCl_2$ $\tilde{A}^1B_1$ + Cl_2	7.3	
		$GeCl_2$ $\tilde{a}^3B_1$ + Cl_2	6.3	
		$GeCl_2$ $\tilde{X}^1A_1$ + 2Cl	6.0	
		$GeCl_2$ $\tilde{X}^1A_1$ + Cl_2	3.5	
		$GeCl_3$ + Cl	2.8	
$GeCl_4$	$\tilde{X}^1A_1$			0

[a] Smith et al. [19].
[b] Threshold for fluorescence is 19.4 ± 0.2 eV (see Section 4.3 of text).
[c] Threshold for fluorescence is 19.0 ± 0.2 eV (see Section 4.3 of text).
[d] Spin–orbit doublet [19].
[e] Energies of the $\tilde{A}^1B_1$ and $\tilde{a}^3B_1$ states of $GeCl_2$ above the $\tilde{X}^1A_1$ ground state from Karolczak et al. [30].

known from experiments, nor are the positions of higher valence or Rydberg states of CCl_2, $SiCl_2$ or $GeCl_2$. The A–X band system of CCl is extremely well characterised [42], but SiCl and GeCl are not observed in this work. The energies of excited states of Si* and Ge* atoms are well known [43], whereas emission in atomic carbon is not observed. Finally, we should note that non-resonant emission from the $\tilde{C}^2T_2$ third excited state of $SiCl_4^+$ and $GeCl_4^+$ has been observed, initially by us [14] but now by others [18, 20], with thresholds at the AIE of this state of $SiCl_4^+$ and $GeCl_4^+$ of 15.0 and 14.6 eV, respectively.

4. Results

4.1. CCl_4

The flux-normalised fluorescence excitation spectrum of CCl_4 recorded at a resolution of 0.4 nm at Daresbury is shown in Fig. 1(a). Peaks are observed between 9 and 13 eV and (very weakly) at 16 eV. Their shape is characteristic of a dissociative process, where the initially populated Rydberg state of the neutral molecule (pre-)dissociates to a fluorescing fragment. Thus for each peak the fluorescence signal increases from threshold, reaches a maximum at the Franck–Condon maximum of the Rydberg state, and recedes to the baseline. The shape of such resonant peaks is most clearly seen for the peaks at 9.42, 9.70 and 11.08 eV. From this spectrum it is not possible to say whether the Rydberg states are repulsive or predissociated bound states. The spectrum is virtually unchanged both in the absolute and relative intensities of the peaks when a Schott GG395 filter is placed in front of the photomultiplier tube (Fig. 1(b)). This implies that the majority of the emission for excitation energies in the range 9–13 eV lies at $\lambda > 380$ nm. In confirmation of this observation, the spectrum disappears when a UG5 filter (transmitting 250–400 nm

only) is used. Fig. 1(c) shows the action spectrum recorded at Bessy with a resolution of 0.3 nm when the secondary monochromator is set to detect only 278 ± 4 nm, corresponding to CCl $A^2\Delta$–$X^2\Pi$ emission. A broad resonant peak at 16 eV, threshold 14.2 ± 0.1 eV, is observed. This value of λ_2 was determined by choosing a suitable peak in the dispersed emission spectra (Fig. 2(c)), and as such was recorded *after* the dispersed spectra measurements had been made. However, for convenience we show this action spectrum in the same figure as the fluorescence excitation spectra, since in all cases it is the primary monochromator that is scanned. Note that the experimental threshold for CCl $A^2\Delta$ production, 14.2 ± 0.1 eV, agrees well with the thermochemical threshold for production of CCl $A^2\Delta$ + 3Cl of 14.32 eV (Table 1).

Dispersed emission spectra (Fig. 2) were recorded at Bessy with the H20UV secondary monochromator and EMI 9789 QB photomultiplier tube with a resolution of 4 nm for VUV excitation energies of 9.7, 11.1 and 16.0 eV. The spectra at energies below 13 eV are dominated by a broad band between 420 and ca. 550 nm. There is some evidence that as E_1 increases the peak in the band (ca. 460–500 nm) moves to slightly lower wavelength. These spectra are in good agreement with those obtained by the groups of Ibuki [8] and Tsuji [13] who used a variety of VUV discharge lamp or metastable atom sources. The emission is assigned by these groups and by us to $CCl_2\,\tilde{A}^1B_1$–$\tilde{X}^1A_1$, although this assignment has been disputed by Breitbarth and Berg [44] who suggest that the emission may be due to CCl_3. There is a small peak at 255 nm in the spectrum with E_1 = 11.1 eV (Fig. 2(b)) which may be due to $Cl_2\,D'$–A' emission. It is not possible to say whether this is caused by first- or second-order radiation from the primary monochromator; the former possibility is energetically allowed (Table 1). No signal is observed between

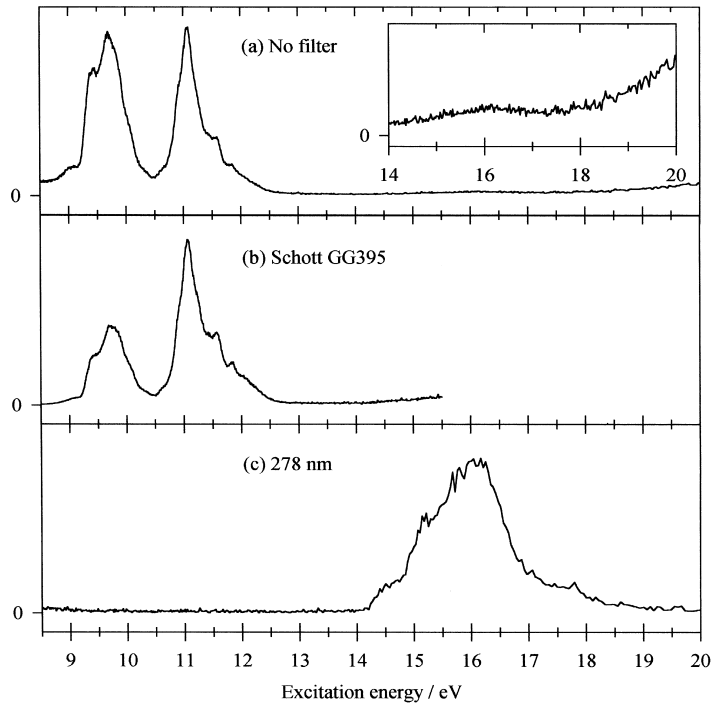

Fig. 1. Fluorescence excitation spectra of CCl_4 between 9 and 20 eV recorded at the Daresbury synchrotron source with a 1 m Seya-Namioka monochromator at an optical resolution of 0.4 nm. The spectra have been flux normalised, and the background subtracted. In (b), a Schott GG395 filter is used in front of the EMI 9813 QB photomultiplier tube. The effective range over which fluorescence is collected is therefore (a) 190–650 and (b) 380–650 nm. (c) Action spectrum of CCl_4 recorded at Bessy 1 between 9 and 20 eV with detection of the fluorescence at 278 ± 4 nm, corresponding to CCl $A^2\Delta$–$X^2\Pi$ emission. The optical resolution is 0.3 nm. Now fluorescence has not been normalised to the vacuum–UV radiation from the primary monochromator.

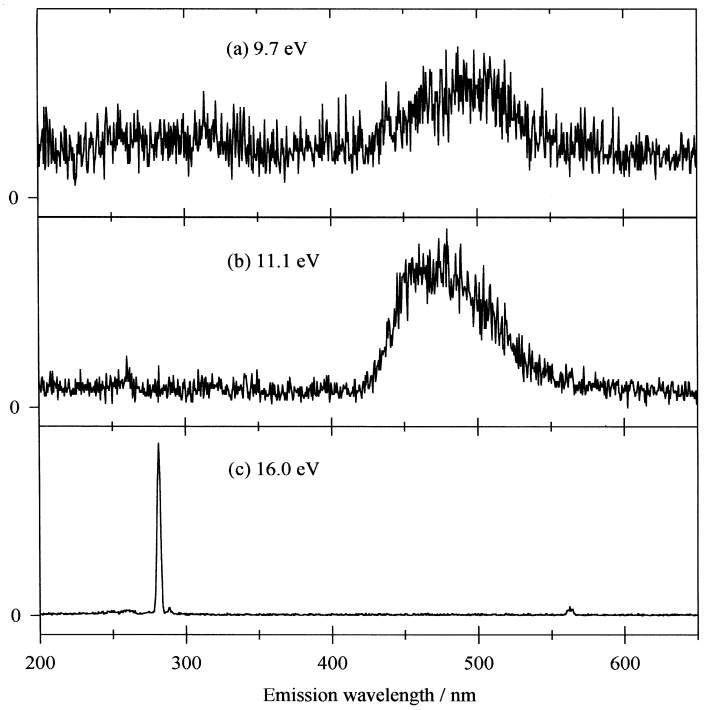

Fig. 2. Dispersed emission spectra recorded at the Bessy 1 synchrotron source for CCl_4 photoexcited at (a) 9.7, (b) 11.1 and (c) 16.0 eV. A Jobin Yvon H20UV was used as the secondary monochromator with a resolution of 4 nm. No attempt has been made to correct for the sensitivity of the secondary monochromator as a function of wavelength.

200 and 250 nm, the range of wavelengths where absorption of CCl_3 from its ground state to the 3*s* Rydberg state occurs [35, 36]. We conclude either that photodissociation of CCl_4 at these energies does not produce CCl_3, or that the branching ratio to this excited state of the radical is very small, or that this low-lying Rydberg state of CCl_3 has a negligibly small fluorescence quantum yield. This can be

Table 4
Peak positions and assignments from fluorescence excitation spectroscopy of the Rydberg states of CCl_4 in the range 9–20 eV that lead to fluorescence, and assignments of the fluorescing fragments

E (eV)	Assignment	(IE − *E*) (eV)	(n − δ)	δ[a]	Emission range (nm)	Emitter	Comment
9.05	$(3t_2)^{-1}4s$	3.46	1.98	2.02	420–ca. 600[b]	$CCl_2\,\tilde{A}^1B_1$	shoulder
9.42	$(1t_1)^{-1}4p$	2.22	2.47	1.53	420–ca. 600	$CCl_2\,\tilde{A}^1B_1$	
9.70	$(3t_2)^{-1}4p$	2.81	2.20	1.80	420–ca. 600	$CCl_2\,\tilde{A}^1B_1$	
11.08	$(1e)^{-1}4p$	2.29	2.43	1.56	420–ca. 600	$CCl_2\,\tilde{A}^1B_1$	
11.58	$(3t_2)^{-1}4d$	0.93	3.82	0.18			
	or $(3t_2)^{-1}5p$	0.93	3.82	1.18	420–ca. 600	$CCl_2\,\tilde{A}^1B_1$	shoulder
11.86	$(3t_2)^{-1}5d$	0.65	4.57	0.43			
	or $(3t_2)^{-1}6p$	0.65	4.57	1.43	420–ca. 600	$CCl_2\,\tilde{A}^1B_1$	shoulder
16.1[c]					276–280	$CCl\,A^2\Delta(v')$	

[a] Quantum defect, δ, defined by the equation $E = \mathrm{IE} - [R_H/(n-\delta)^2]$, where R_H is the Rydberg constant and n is the principal quantum number of the Rydberg orbital. Calculated using the appropriate vertical ionisation potentials for CCl_4 from photoelectron spectroscopy [24].

[b] Maximum in the fluorescence at ca. 480 nm.

[c] Threshold for fluorescence is 14.2 ± 0.1 eV.

contrasted with the CF_3 radical where strong UV and visible emission bands produced by photodissociation of low-lying Rydberg states of CF_3-containing molecules are well characterised [4]. For an excitation energy of 16.0 eV (Fig. 2(c)), the dispersed emission spectrum changes dramatically. The CCl_2 $\tilde{A}$–$\tilde{X}$ band disappears, to be replaced by a narrow band at 278 which is assigned to CCl $A^2\Delta$–$X^2\Pi$. These results and the assignments of the CCl_4 Rydberg states will be discussed in Section 5. They are summarised in Table 4.

The CCl_2 $\tilde{A}$-state lifetime has been measured both in the gas phase [8, 45] and in an argon matrix [46] to be in the microsecond range. It is therefore too long to measure using the single-bunch mode of Bessy, and confirm the identity of the emitter. We have, however, measured the lifetime of the CCl $A^2\Delta$ state, produced by VUV photodissociation of CCl_4 with $E_1 = 16$ eV and $\lambda_2 = 278$ nm. The decay fits to a single exponential decay with $\tau = 53 \pm 2$ ns (Table 7). We should note that our experiment affords no selectivity on the CCl $A^2\Delta$ vibrational states produced by VUV photodissociation of CCl_4, so this value is an average over the range of vibrational levels of CCl $A^2\Delta$ that fluoresce.

4.2. $SiCl_4$

Fig. 3 shows fluorescence excitation spectra of $SiCl_4$ recorded at Daresbury at a resolution of 0.4 nm. The three spectra were obtained with (a) no filter, (b) a Schott UG5 and (c) a Schott GG395 in front of the photomultiplier tube. The effective range over which fluorescence is collected is therefore (a) 190–650, (b) 250–400 and (c) 380–650 nm. Resonant peaks are observed between 11 and 14 eV, three particularly strong features being observed at 11.45, 12.10 and 12.88 eV. Since the vertical IE to the ground state of $SiCCl_4^+$ is only 12.1 eV [19], the two latter features must arise from Rydberg states converging on excited states of $SiCl_4^+$. The most pertinent point to note is that the lowest-energy peak at 11.45 eV has a higher intensity relative to that of the two other peaks when visible radiation only is transmitted through the Schott GG395 filter. This peak is absent with the UG5 UV filter. This means that fluorescence caused by the photodissociation of these Rydberg states is most likely to occur in the visible for the peak at 11.45 eV, but in the UV for the peaks at 12.10 and 12.88 eV. We show later that these emissions are due to the $\tilde{a}^3B_1$–$\tilde{X}^1A_1$ (origin 534 nm [40]) and $\tilde{A}^1B_1$–$\tilde{X}^1A_1$ (origin 333 nm [28]) bands of $SiCl_2$, respectively. At higher excitation energies, a non-resonant peak is observed with a threshold of 15.0 ± 0.1 eV. The shape and greater width of the peak are characteristic of fluorescence from an excited state of the parent molecular ion, and this energy agrees exactly with the adiabatic IE of the $(2t_2)^{-1}\tilde{C}^2T_2$ state of $SiCl_4^+$. The filter experiments show that the majority of the emission from this state occurs in the visible at $\lambda > 400$ nm; with the Schott GG395 filter, the relative intensity of this peak increases substantially compared with the $SiCl_2$ $\tilde{A}$–$\tilde{X}$ UV bands caused by photodissociation of $SiCl_4$ at 12.1 and 12.9 eV. This confirms results from electron-impact studies which have shown that emission from the $\tilde{C}^2T_2$ state of $SiCl_4^+$ occurs both to the $\tilde{X}^2T_1$ ground and the $\tilde{A}^2T_2$ first excited states, with peak wavelengths of the two broad bands of ca. 410 and 560 nm [14]. At an energy of 16.65 eV, the first member of a weak series of peaks converging on the $(2a_1)^{-1}\tilde{D}^2A_1$ fourth excited state of $SiCl_4^+$ is observed. These Rydberg states give rise to resonant peaks in the VUV fluorescence excitation spectrum, and have been observed before [14, 17, 18]. It is believed that these states autoionise to the $\tilde{C}^2T_2$ state of $SiCl_4^+$, and hence are observed in fluorescence.

Fig. 4 shows four dispersed emission spectra recorded at Bessy at the excitation energies of the main peaks in the $SiCl_4$ VUV fluorescence spectrum. Two were recorded with the Jobin Yvon H20UV secondary monochromator plus EMI 9789 QB photomultiplier tube at a resolution of 4 nm, two with the H20VIS plus Hamamatsu R6060 photomultiplier tube at a resolution of 8 nm. Full details are given in the caption. The former detection system has the maximum in its sensitivity at wavelengths below 400 nm, the latter at wavelengths above 400 nm. Interpretation of these spectra is further complicated by the presence of second-order radiation from the primary monochromator for $\lambda_1 > \sim 100$ nm ($E_1 <$ 12.4 eV) [2–6]. Fig. 4(c) shows a ''clean'' spectrum of the $SiCl_4^+$ $\tilde{C}$–$\tilde{X}$ and $\tilde{C}$–$\tilde{A}$ bands for $E_1 = 15.9$ eV, above the energy of the $SiCl_4^+$ $\tilde{C}^2T_2$ adiabatic IE and that where second-order effects are important. Two broad bands are observed at 410 and 560 nm, peak

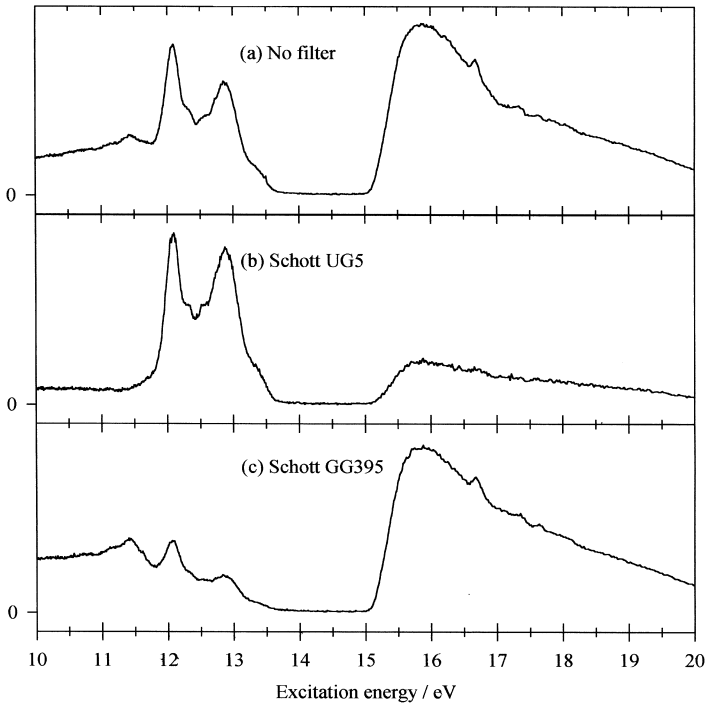

Fig. 3. Fluorescence excitation spectra of $SiCl_4$ between 10 and 20 eV recorded at the Daresbury synchrotron source (Seya 1 m monochromator) with a resolution of 0.4 nm. The spectra have been flux normalised, and the background subtracted. In (b) and (c), Schott UG5 and GG395 filters, respectively, are used in front of the EMI 9813 QB photomultiplier tube. The effective range over which fluorescence is collected is therefore (a) 190–650, (b) 250–400 and (c) 380–650 nm.

heights being in the ratio ca. 3:2. For $E_1 = 11.4$ eV (Fig. 4(a)) recorded with the same ''visible'' detection system, the same two broad bands are observed, but the higher-wavelength band now has comparable intensity. This strongly suggests that, in addition to $SiCl_4^+$ $\tilde{C}$–$\tilde{X}$ and $\tilde{C}$–$\tilde{A}$ bands being observed due to second-order radiation at 22.8 eV, the $SiCl_4$ Rydberg state at 11.45 eV gives rise to fluorescence around 500–600 nm. This emission is the $SiCl_2$ $\tilde{a}^3B_1$–$\tilde{X}^1A_1$ band system [40, 29], although one cannot discount totally a contribution from an unknown emission band in the $SiCl_3$ radical; existing ab initio calculations on this radical are limited to properties of its *ground* electronic state [47]. For $E_1 = 12.1$ eV (Fig. 4(b)) recorded with the ''UV'' detection system, a new band peaking at 320 nm is observed. This band is due to $SiCl_2$ $\tilde{A}^1B_1$–$\tilde{X}^1A_1$ [28], and suggests that the $SiCl_4$ Rydberg states at 12.10 and 12.88 eV photodissociate via this channel. For $E_1 = 24.8$ eV (Fig. 4(d)), sharp atomic lines due to Si are observed between 200 and 300 nm, as well as the molecular bands due to emission from $SiCl_4^+$ $\tilde{C}^2T_2$. Five lines are observed at 213, 222, 248, 253 and 289 nm. They are assigned to the following transitions in atomic Si [43]: $^1P_1$–^3P, ^3D–^3P, $^1P_1$–^3P, ^3P–^3P and $^1P_1$–$^1D_2$. The first four emission lines involve transitions to the ground state (^3P) of the Si atom, and it is noted that the weak lines at 213 and 248 nm are spin-forbidden transitions whereas the stronger lines at 222, 253 and 289 nm are spin-allowed. Since the spin–orbit splittings of the triplet states of Si are relatively small, the observed triplet transitions cannot be assigned to individual spin–orbit components. These results, to be discussed in Section 5, are summarised in Table 5.

Action spectra recorded at λ_2 values of 255, 320 and 410 nm are shown in Fig. 5. These wavelengths correspond to the following emissions: (a) Si ^3P–^3P, (b) $SiCl_2$ $\tilde{A}^1B_1$–$\tilde{X}^1A_1$ and (c) $SiCl_4^+$ $\tilde{C}^2T_2$–$\tilde{X}^2T_1$. The threshold for Si* ^3P production is 21.8 ± 0.2 eV (ignoring the weak peak caused by second-order

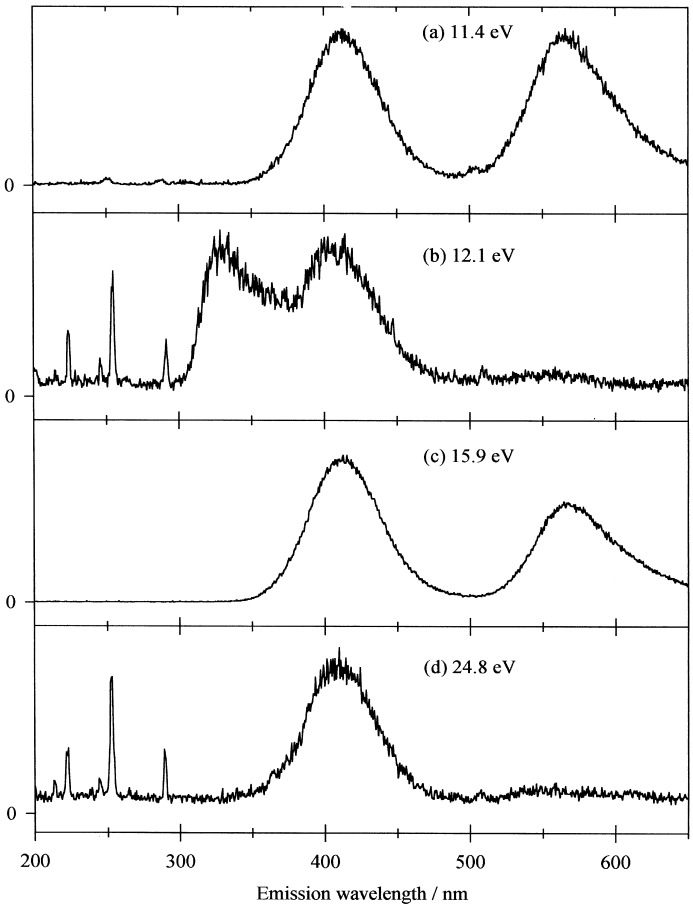

Fig. 4. Dispersed emission spectra recorded at the Bessy 1 synchrotron source for $SiCl_4$ photoexcited at (a) 11.4, (b) 12.1, (c) 15.9 and (d) 24.8 eV. A Jobin Yvon H20VIS was used as the secondary monochromator at a resolution of 8 nm plus a Hamamatsu R6060 photomultiplier tube for (a) and (c), an H20UV at a resolution of 4 nm plus an EMI 9789 QB photomultiplier tube for (b) and (d). (a) and (b) show clearly the extended visible ($\lambda > 400$ nm) and UV ($\lambda < 400$ nm) sensitivities of the two detection systems. No attempt has been made to correct for the sensitivity of either secondary monochromator as a function of wavelength.

radiation at a threshold of 10.9 eV), and we note that this energy agrees fairly well with the thermochemical threshold to produce this excited state of Si with four Cl atoms of 21.4 eV (Table 2). The threshold for $SiCl_2$ $\tilde{A}^1B_1$ production is 11.8 ± 0.2 eV. This energy is above that of the lowest Rydberg state observed in this work at 11.45 eV, suggesting that this Rydberg state photodissociates exclusively to the $\tilde{a}^3B_1$ triplet state of $SiCl_2$. This 320 nm action spectrum, however, suggests that the 12.10 and 12.88 eV Rydberg states photodissociate via the $SiCl_2$ $\tilde{A}^1B_1$ singlet channel; it is not possible to say whether this is a minor or the dominant channel compared with photodissociation via the $\tilde{a}^3B_1$ triplet channel. The main threshold for emission at 410 nm occurs at 15.0 ± 0.1 eV, the adiabatic IE of the $\tilde{C}^2T_2$ state of $SiCl_4^+$. The weak signal between 10.5 and 12.5 eV is due to second-order radiation at 21–25 eV also producing, non-resonantly, the $SiCl_4^+$ $\tilde{C}^2T_2$ state.

Lifetime decays were measured for several values of E_1 and λ_2 shown in Table 7. Decays from (a) the $\tilde{A}^1B_1$ state of $SiCl_2$, (b) the $\tilde{C}^2T_2$ state of $SiCl_4^+$, (c) the ^3P and (d) the ^3D excited states of the Si atom are shown in Fig. 6. The important results (all tabulated in Table 7) are that the $SiCl_2$ $\tilde{A}^1B_1$ state has a lifetime of 67 ± 9 ns (this value being an average over all the

Table 5
Peak positions and assignments from fluorescence excitation spectroscopy of the Rydberg states of $SiCl_4$ in the range 11–17 eV that lead to fluorescence, and assignments of the fluorescing fragments

E (eV)[a]	Assignment	(IE − E) (eV)	(n − δ)	δ[b]	Emission range (nm)	Emitter	Comment
11.45	$(1e)^{-1}4p$	2.05	2.57	1.43	$\lambda > 500$[c]	$SiCl_2\ \tilde{a}^3B_1$	
12.10	$(3t_2)^{-1}4d$	0.90	3.89	0.11	300–420[d]	$SiCl_2\ \tilde{A}^1B_1$	
					$\lambda > 500$[e]	$SiCl_2\ \tilde{a}^3B_1$	
12.3	$(3t_2)^{-1}6p$	0.7	4.41	1.59	300–420	$SiCl_2\ \tilde{A}^1B_1$	Shoulder
					$\lambda > 500$	$SiCl_2\ \tilde{a}^3B_1$	
12.6	$(1e)^{-1}4d$	0.9	3.89	0.11			
	or $(3t_2)^{-1}6d$	0.4	5.83	0.17	300–420	$SiCl_2\ \tilde{A}^1B_1$	Shoulder
					$\lambda > 500$	$SiCl_2\ \tilde{a}^3B_1$	
12.88	$(1e)^{-1}6p$	0.62	4.68	1.32			
	or $(1e)^{-1}5d$	0.62	4.68	0.32	300–420	$SiCl_2\ \tilde{A}^1B_1$	
					(and $\lambda > 500$?)	($SiCl_2\ \tilde{a}^3B_1$)	
13.3	$(2t_2)^{-1}4p$	2.0	2.61	1.39	300–420	$SiCl_2\ \tilde{A}^1B_1$	Shoulder
					(and $\lambda > 500$?)	($SiCl_2\ \tilde{a}^3B_1$)	
15.0[f]	$(2t_2)^{-1} \rightarrow SiCl_4^+\ \tilde{C}^2T_2 + e^-$				350–ca. 650[g]	$SiCl_4^+\ \tilde{C}^2T_2$	
16.65	$(2a_1)^{-1}4p$	1.45	3.06	0.94	350–ca. 650	$SiCl_4^+\ \tilde{C}^2T_2$	

[a] Effects of second-order radiation producing $SiCl_4^+\ \tilde{C}$-state emission at excitation energies less than 15.0 eV are ignored in this table.
[b] Quantum defect, δ, defined by the equation $E = \text{IE} - [R_H/(n - \delta)^2]$, where R_H is the Rydberg constant and n is the principal quantum number of the Rydberg orbital. Calculated using the appropriate vertical ionisation potentials for $SiCl_4$ from threshold photoelectron spectroscopy [19].
[c] Maximum in the fluorescence at ca. 560 nm.
[d] Maximum in the fluorescence at ca. 330 nm.
[e] Maximum in $SiCl_2\ \tilde{a}$–$\tilde{X}$ at ca. 560 nm [40, 29].
[f] Threshold for fluorescence, not peak position.
[g] Lambert et al. [14]. Maxima in the fluorescence at ca. 410 nm ($SiCl_4^+\ \tilde{C}^2T_2$–$\tilde{X}^2T_1$) and 560 nm ($SiCl_4^+\ \tilde{C}^2T_2$–$\tilde{A}^2T_2$).

vibrational levels populated by $SiCl_4$ photodissociation), the $SiCl_4^+\ \tilde{C}^2T_2$ state 37.5 ± 0.4 ns. Both results are in excellent agreement with data from other sources [15, 18, 48]. The Si emissions at 254 and 221 nm show very different time-resolved decays (Figs. 6(c) and 6(d)). The former can only fit to a double exponential with a main component of 4.9 ± 0.2 ns and a weaker component of 49 ± 3 ns. The latter can only fit to a single exponential with a lifetime of 24.3 ± 0.6 ns. These results are discussed in Section 5.

4.3. $GeCl_4$

Fig. 7 shows fluorescence excitation spectra of $GeCl_4$ recorded at Daresbury at a resolution of 0.4 nm. The three spectra were recorded with (a) no filter, (b) a Schott UG5 and (c) a Schott GG455 in front of the EMI 9813 QB photomultiplier tube. Six resonant peaks are observed between 9 and 12 eV. The relative intensities of five of the peaks are unchanged by which filter is used in front of the photomultiplier tube, but the lowest-energy peak at 9.59 eV virtually disappears with the UV-transmitting UG5 filter. Hence the fluorescence caused by photodissociation of this Rydberg state is exclusively in the visible at $\lambda > 400$ nm, whereas the other peaks have both visible and UV components. As with $SiCl_4$, we believe that these emissions are due to $GeCl_2\ \tilde{a}^3B_1$–$\tilde{X}^1A_1$ (origin 448 nm [30]) and $\tilde{A}^1B_1$–$\tilde{X}^1A_1$ (origin 327 nm [30]), respectively. (No theoretical or experimental information is available on excited states of $GeCl_3$ and, in the absence of such data, we must assume that, like CCl_3 and $SiCl_3$, valence states of the radical do not fluoresce.) At higher excitation energies, a non-resonant peak is observed with a threshold at 14.6 ± 0.1 eV. The shape and larger width of the peak is characteristic of fluorescence from an excited state of the parent ion, and this energy agrees exactly with the adiabatic IE of the $(2t_2)^{-1}\tilde{C}^2T_2$ state of $GeCl_4^+$ [19]. The filter experiments show that, compared with the resonant

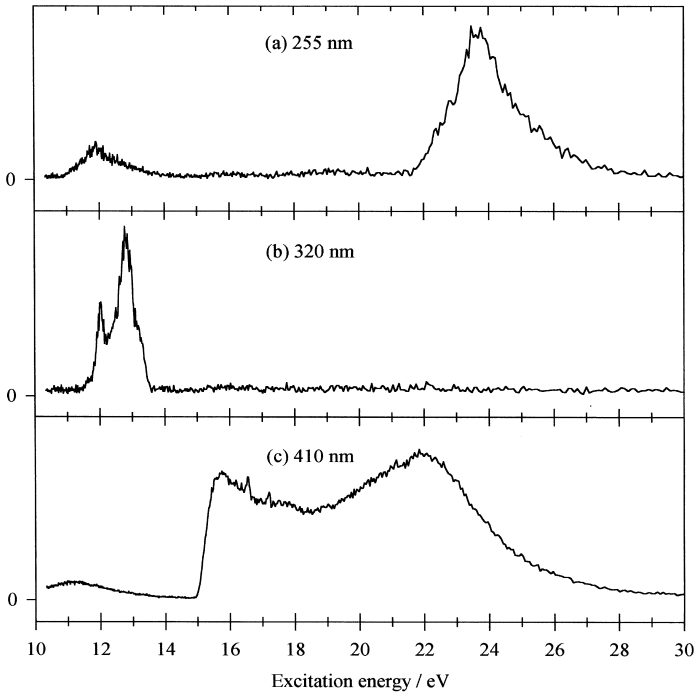

Fig. 5. Action spectra of $SiCl_4$ recorded at the Bessy 1 synchrotron source between 10 and 30 eV with detection of the fluorescence at (a) 255 ± 4, (b) 320 ± 4 and (c) 410 ± 8 nm. These wavelengths correspond primarily to emissions in (a) Si ^3P–^3P, (b) $SiCl_2$ $\tilde{A}^1B_1$–$\tilde{X}^1A_1$ and (c) $SiCl_4^+$ $\tilde{C}^2T_2$–$\tilde{X}^2T_1$, respectively In all cases, the optical resolution is 0.3 nm, and fluorescence has not been normalised to the vacuum–UV radiation from the primary monochromator. A Jobin Yvon H20UV secondary monochromator was used for (a) and (b), an H20VIS for (c).

peaks between 9 and 12 eV, the majority of the emission from this state occurs in the visible at $\lambda >$ 400 nm; the threshold at 14.6 eV disappears with the UG5 UV-transmitting filter but it dominates the resonant peaks with the GG455 visible-transmitting filter. As with $SiCl_4$, this result has been confirmed by electron-impact studies which have shown that emission from the $\tilde{C}^2T_2$ state of $GeCl_4^+$ occurs both to the $\tilde{X}^2T_1$ and the $\tilde{A}^2T_2$ first excited state of the parent ion, with peak wavelengths of the two broad bands of ca. 490 and 620 nm [14].

Fig. 8 shows three dispersed emission spectra recorded with a resolution of 4 nm at excitation energies of 10.0, 16.1 and 20.0 eV using the Jobin Yvon H20UV plus EMI 9789 QB photomultiplier tube at Bessy. The spectrum at 10.0 eV (Fig. 8(a)) was recorded with the LiF window in front of the exit slit of the primary monochromator, ensuring no second-order radiation (at 20.0 eV) was present. It is dominated by a broad band between 400 and 520 nm, peaking at ca. 460 nm. Emission is due to the $\tilde{a}^3B_1$–$\tilde{X}^1A_1$ band of $GeCl_2$, and the only surprise is the virtual absence of the band at 327 nm due to $GeCl_2$ $\tilde{A}^1B_1$–$\tilde{X}^1A_1$; the Daresbury spectrum recorded with a UG5 filter (Fig. 7(b)) shows that emission from the $GeCl_4$ Rydberg state at 10 eV *does* lead to emission below 400 nm. We conclude that whereas the Rydberg state at 9.59 eV leads exclusively to production of $GeCl_2$ $\tilde{a}^3B_1$, the five other states between 10 and 12 eV photodissociate predominantly to this state, and the channel to $GeCl_2$ $\tilde{A}^1B_1$ is minor. This conclusion is in agreement with Ibuki and Kamamoto's recent work [20]. The dispersed emission spectrum at 16.1 eV (Fig. 8(b)) is dominated by a single broad band covering the same wavelength range as the $GeCl_2$ $\tilde{a}$–$\tilde{X}$ emission. This band is due to $GeCl_4^+$ $\tilde{C}^2T_2$–$\tilde{X}^2T_1$, and the higher-wavelength $\tilde{C}$–$\tilde{A}$ band is not seen due to the rapid reduction in sensitivity of the dispersed detection system for $\lambda_2 >$ 500 nm. We note that the $GeCl_2$ $\tilde{a}$–$\tilde{X}$ and $GeCl_4^+$ $\tilde{C}$–$\tilde{X}$ bands cover a very similar range of wavelengths, so that at the modest resolution at which

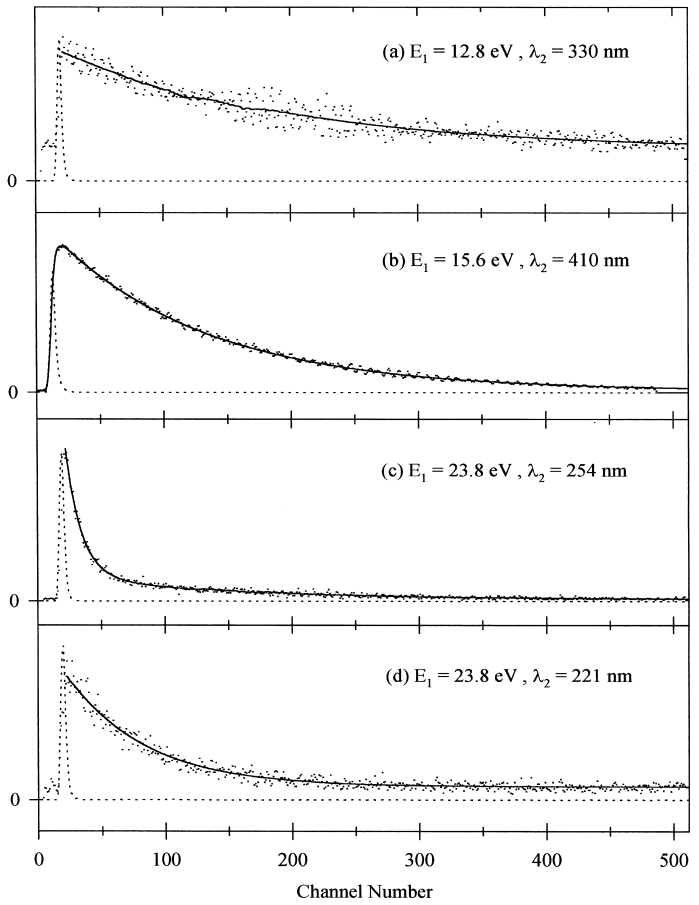

Fig. 6. Decay of the fluorescence following excitation of $SiCl_4$ at (a) 12.8, (b) 15.6, (c) and (d) 23.8 eV with single-bunch, pulsed radiation from the Bessy 1 synchrotron source. The secondary monochromator is set to (a) 330 ± 8, (b) 410 ± 8, (c) 254 ± 8 and (d) 221 ± 8 nm, respectively. Each spectrum shows the experimental data points, the prompt signal (dashed line), and the fit to the data (solid line) using the method described in Section 2 and [23]. The time calibration is 0.395 ns per channel in (a), (c) and (d), 0.312 ns per channel in (b). The emitters are (a) $SiCl_2$ $\tilde{A}^1B_1$, (b) $SiCl_4^+$ $\tilde{C}^2T_2$, (c) Si* $^3P_1$ and (d) Si* $^3D_1$. (a), (b) and (d) fit to single-exponential functions with lifetimes of 67 ± 9, 37.5 ± 0.4 and 24.3 ± 0.6 ns, respectively. (c) can only fit satisfactorily to a double-exponential function with lifetimes of 4.9 ± 0.2 and 49 ± 3 ns.

dispersed spectra are recorded it is impossible to differentiate the two emissions. (This was not the case with $SiCl_4^+$ $\tilde{C}$–$\tilde{X}$ and $SiCl_2$ $\tilde{a},\tilde{A}$–$\tilde{X}$ emissions, and consequently made the $SiCl_4$ dispersed emission spectra much easier to interpret.) The dispersed spectrum at 20.0 eV (Fig. 8(c)) shows the same $GeCl_4^+$ $\tilde{C}$–$\tilde{X}$ band, observed at an energy well above its threshold because the process is non-resonant, and, in addition, Ge atomic lines below 350 nm. The two strongest lines at 267 and 307 nm are the analogous $^3P_1$–$^3P_0$ and $^1P_1$–$^1D_2$ transitions [43] to those observed in atomic Si at 253 and 289 nm (Section 4.2). The three weaker lines observed at 260, 272 and 277 nm are assigned to $^1P_1$–$^1D_2$ or $^3P_2$–$^3P_1$, $^3P_0$–$^3P_1$ and $^3P_{0,1}$–$^3P_2$, respectively. Action spectra were recorded at λ_2 values of 267, 307 and 470 nm. The third value of λ_2 corresponds to the $GeCl_4^+$ $\tilde{C}$–$\tilde{X}$ molecular band. Thresholds were observed at 19.0 ± 0.2, 19.4 ± 0.2 and 14.6 ± 0.1 eV. We note that the experimental thresholds for Ge* $^3P_1$ and $^1P_1$ production agree well with the calculated thermochemical energy of these two excited states of Ge produced with four Cl atoms of 18.8 and 19.1 eV, respectively (Table 3). These results, to be discussed in Section 5, are summarised in Table 6.

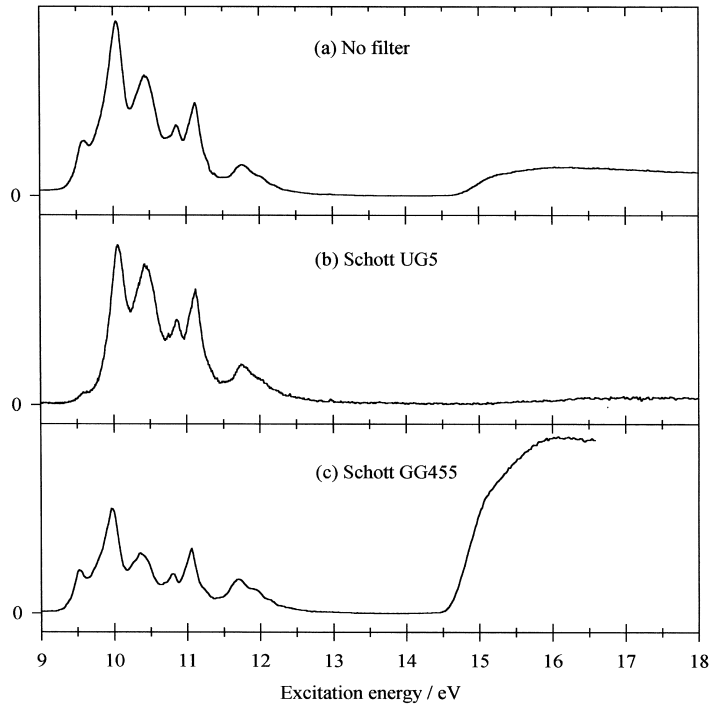

Fig. 7. Fluorescence excitation spectra of $GeCl_4$ between 9 and 18 eV recorded at the Daresbury synchrotron source. (a) and (b) were recorded with the 1 m Seya monochromator at a resolution of 0.4 nm, (c) with the 5 m McPherson monochromator at a resolution of 0.2 nm. The spectra have been flux normalised, and the background subtracted. In (b) and (c), Schott UG5 and GG455 filters, respectively, are used in front of the EMI 9813 QB photomultiplier tube. The effective range over which fluorescence is collected is therefore (a) 190–650, (b) 250–400 and (c) 440–650 nm.

Lifetime decays were measured for several values of E_1 and λ_2, and the results are shown in Table 7. The lifetime of the $GeCl_4^+$ $\tilde{C}^2T_2$ state ($E_1 = 16.1$ eV, $\lambda_2 =$ 470 nm) is measured to be 65 ± 4 ns, in excellent agreement with an earlier single-bunch measurement of 65.4 ± 0.4 ns [15]. The results for $E_1 = 10.0$ eV are the most interesting. For $\lambda_2 = 470$ nm and hence the detection system isolating the $GeCl_2$ $\tilde{a}^3B_1$–$\tilde{X}^1A_1$ emission, the experimental decay in signal is absolutely flat over the multi-channel analyser. With the excellent signal-to-noise ratio of this spectrum, we assume that a flat decay over the lifetime of the experiment (208 ns) implies a radiative lifetime of the emitter of greater than ca. 500 ns. This is compatible with Ibuki's measurement of 17.4 μs for the lifetime of this emission [39] which, at the time, he assigned to the lifetime of $GeCl_2$ $\tilde{A}^1B_1$. Following Karolczak et al.'s rotational analysis of both this and the 327 nm band, there seems little doubt that Ibuki's assignment is incorrect, and the 470 nm band is due to the spin-forbidden $\tilde{a}$–$\tilde{X}$ transition in $GeCl_2$, an assignment with which Ibuki et al. now agree in their most recent VUV fluorescence study on $GeCl_4$ [20]. Assuming that this value of 17.4 μs is correct, it is perhaps surprising that the lifetime of this state is so long, given both the apparent strength of the $\tilde{a}$–$\tilde{X}$ emission in $GeCl_2$ and the much lower lifetime (355 ± 8 ns [18]) for the analogous $\tilde{a}^3B_1$ state of $SiCl_2$. For $E_1 = 10.0$ eV, $\lambda_2 = 325$ nm and hence isolating the $GeCl_2$ $\tilde{A}^1B_1$–$\tilde{X}^1A_1$ emission, there is a small but definite decay in the time-resolved fluorescence signal over the lifetime of the experiment. We therefore estimate the lifetime of the $\tilde{A}^1B_1$ state to lie in the range ca. 100–500 ns. This value is compatible with Ibuki's measurement of 90 ± 7 ns [39], which he assigned (incorrectly) to that of the second excited singlet valence state of $GeCl_2$, $\tilde{B}^1A_2$. The results for $E_1 =$ 21 eV are particularly revealing of the power of this

Table 6
Peak positions and assignments from fluorescence excitation spectroscopy of the Rydberg states of $GeCl_4$ in the range 9–15 eV that lead to fluorescence, and assignments of the fluorescing fragments

E (eV)[a]	Assignment	(IE − E) (eV)	(n − δ)	δ[b]	Emission range (nm)	Emitter(s)
9.59	$(1t_1)^{-1}4p$	2.51	2.33	1.67	420–530[c]	$GeCl_2$ $\tilde{a}^3B_1$
10.04	$(3t_2)^{-1}4p$	2.63	2.27	1.73	420–530	$GeCl_2$ $\tilde{a}^3B_1$
					(300–330)	($\tilde{A}^1B_1$)
10.42	$(1e)^{-1}4p$	2.68	2.25	1.75	420–530	$GeCl_2$ $\tilde{a}^3B_1$
					(300–330)	($\tilde{A}^1B_1$)
10.86	$(1t_1)^{-1}5p$	1.24	3.31	1.69	420–530	$GeCl_2$ $\tilde{a}^3B_1$
					(300–330)	($\tilde{A}^1B_1$)
11.07	$(3t_2)^{-1}5s$	1.60	2.91	2.09	420–530	$GeCl_2$ $\tilde{a}^3B_1$
					(300–330)	($\tilde{A}^1B_1$)
11.77	$(1e)^{-1}5p$	1.33	3.20	1.80	420–530	$GeCl_2$ $\tilde{a}^3B_1$
					(300–330)	($\tilde{A}^1B_1$)
14.6[d]	$(2t_2)^{-1} \rightarrow GeCl_4^+$ $\tilde{C}^2T_2 + e^-$				400–ca. 800[e]	$GeCl_4^+$ $\tilde{C}^2T_2$

[a] Effects of second-order radiation producing $GeCl_4^+$ $\tilde{C}$-state emission at excitation energies less than 14.6 eV are ignored in this table.
[b] Quantum defect, δ, defined by the equation $E = \mathrm{IE} - [R_H/(n - \delta)^2]$, where R_H is the Rydberg constant and n is the principal quantum number of the Rydberg orbital. Calculated using the appropriate vertical ionisation potentials for $GeCl_4$ from threshold photoelectron spectroscopy [19].
[c] Maximum in the fluorescence at ca. 460 nm.
[d] Threshold for fluorescence, not peak position.
[e] Lambert et al. [14], Ibuki and Kamamoto [20]. Maxima in the fluorescence at ca. 490 nm ($GeCl_4^+$ $\tilde{C}^2T_2$–$\tilde{X}^2T_1$) and 620 nm ($GeCl_4^+$ $\tilde{C}^2T_2$–$\tilde{A}^2T_2$).

technique to measure radiative lifetimes. If the secondary monochromator is set to either 0 or 470 nm, hence defining the dominant integrated emission at this VUV energy of $GeCl_4^+$ $\tilde{C}$–$\tilde{X}$, the lifetime of the $GeCl_4^+$ $\tilde{C}^2T_2$ state is measured, and a value of 65.9 ± 1.4 ns is obtained, in excellent agreement with our published value [15]. If, however, λ_2 is set to either 267 or 305 nm to define a narrow Ge atomic line, lifetimes of the atomic lines only are measured. These lifetimes would be very difficult to measure without the ability to monochromatise and disperse the induced fluorescence. As with the analogous Si atomic lines at 253 and 289 nm (4.2), these two decays can only fit to double-exponential functions with a main short component of ca. 4.5 ± 0.1 ns and a weaker longer component of ca. 40 ± 2 ns.

5. Discussion

First, it is appropriate to make some general comments about the assignments of the Rydberg spectra. The resonant peaks (of energy E) observed are due to absorption to Rydberg states of MCl_4 which photodissociate to a fluorescing state of a neutral fragment. The assignment of the Rydberg transition relies upon the ionisation energies (IE) of the state of the parent ion to which the Rydberg state converges through the well-known formula

$$E = \mathrm{IE} - \frac{R_H}{(n - \delta)^2} \quad (4)$$

where R_H is the Rydberg constant, and δ is the quantum defect of the Rydberg orbital of principal quantum number n to which an electron in MCl_4 has been promoted. There has been inconsistency in the literature whether to use adiabatic or vertical IEs in such calculations. Causley and Russell [7] use vertical IEs for the $(1t_1)^{-1}$, $(3t_2)^{-1}$ and $(1e)^{-1}$ photoelectron bands of MCl_4. Ibuki et al.'s early work on CCl_4 [8] used vertical IEs established by Green et al. [50], whereas their later work on $SiCl_4$ and $GeCl_4$ [18, 20] used adiabatic IEs from threshold photoelectron spectroscopy [19]. For large values of n, corresponding to small values of (IE − E), which value of IE is used can make a substantial difference to the assignment of the Rydberg state and hence its quantum defect. In this work, as in our previous

Table 7
Lifetimes of emission bands observed from vacuum–UV excitation of CCl_4, $SiCl_4$ and $GeCl_4$ in the range 9–25 eV

Molecule	E_1 (eV)	λ_2 (nm)	τ_n (ns)	A_n	Reduced χ^2	Emitter(s)
CCl_4	16.0	278	53 ± 2[a]		3.7	CCl $A^2\Delta(v = 0,1,2)$[a]
$SiCl_4$	12.8	330	67 ± 9		4.7	$SiCl_2$ $\tilde{A}^1B_1$[b]
	12.8[c]	410	40.6 ± 1.1		1.1	$SiCl_4^+$ $\tilde{C}^2T_2$
	15.6	410	37.5 ± 0.4		3.7	$SiCl_4^+$ $\tilde{C}^2T_2$
	23.8	0	37.0 ± 0.3		1.6	$SiCl_4^+$ $\tilde{C}^2T_2(+Si^*)$
	23.8	221	24.3 ± 0.6[d]		1.1	Si* ^3D
	23.8	254	4.9 ± 0.2[e]	1.0 ± 0.2	1.2	Si* ^3P
			49 ± 3	0.04 ± 0.01		
	23.8	289	4.1 ± 0.2[e]	1.0 ± 0.1	1.1	Si* $^1P_1$
			48 ± 6	0.09 ± 0.01		
$GeCl_4$	10.0	325	long[f]			$GeCl_2$ $\tilde{A}^1B_1$
	10.0	470	flat decay[g]			$GeCl_2$ $\tilde{a}^3B_1$
	16.1	470	65 ± 4		6.4	$GeCl_4^+$ $\tilde{C}^2T_2$
	21.0	267	4.7 ± 0.1[e]	1.0 ± 0.1	1.6	Ge* $^3P_1$
			42 ± 2	0.03 ± 0.01		
	21.0	305	4.4 ± 0.1[e]	1.0 ± 0.1	1.2	Ge* $^1P_1$
			37 ± 2	0.02 ± 0.01		
	21.0	470	65.9 ± 1.4		1.7	$GeCl_4^+$ $\tilde{C}^2T_2$

[a] Average lifetime for the vibrational levels of CCl $A^2\Delta$ that lie below the barrier in the calculated potential energy surface and fluorescence ($v' = 0,1,2$) [49].
[b] Ibuki et al. [18] obtain 73 ± 2 ns, Suzuki et al. [48] 77 ± 3 ns.
[c] In effect, second-order radiation at 25.6 eV in this experiment.
[d] Poor fit to a double-exponential function.
[e] Poor fit to a single-exponential function.
[f] Definite fall in signal over the lifetime of the experiments (208 ns), but the lifetime of the emitter is too long to measure with a repetition rate of 4.8 MHz. We estimate $100 < \tau < 500$ ns. Compatible with Ibuki's measurement of 90 ± 7 ns [39].
[g] With the single-to-noise ratio of our spectra, we assume that a flat decay over the lifetime of the experiment (208 ns) implies $\tau >$ ca. 500 ns. Compatible with Ibuki's measurement of 17.4 ± 0.6 μs [39].

studies [2–6], we use *vertical* IEs for two reasons. First, no resolved vibrational structure is observed in any of the Rydberg transitions, so each band represents a convolution of many vibrational components all with an appropriate Franck–Condon factor. Since there is negligible change in geometry between a Rydberg state and the state of the parent ion to which it converges, the peak of an unresolved photoelectron band will also correspond to the maximum in the Franck–Condon-weighted vibrational envelope, i.e., the vertical IE. (Note that this is not strictly true if non-Franck–Condon effects, such as autoionisation, are prevalent in the photoionisation process.) Under these circumstances, it seems appropriate to assign peak positions in the Rydberg spectra by their convergence on the vertical IE of the parent ion. Second, the adiabatic IE in a vibrationally-unresolved photoelectron band is generally taken to be the energy at which the signal rises above the background (i.e., the first onset), whereas strictly the AIE corresponds to the transition from $v = J = 0$ of the neutral molecule to $v = J = 0$ of the cation. If Franck–Condon factors at threshold are very low, the first onset can appear at a higher energy than the true adiabatic IE. Conversely, for room temperature experiments in which the Franck–Condon factor for photoionisation to $v^+ = 0$ is large, the thermal energy of the neutral molecule may mean that the first onset has a lower energy than the true adiabatic IE. (This latter problem is well documented for photoionisation mass spectrometric studies [51], but seems to be discussed less often in the context of photoelectron spectroscopy.) In either case, it therefore seems unwise to use first onsets as representing the adiabatic IE in a vibrationally-unresolved photoelectron band. It is for these two reasons that, in the context of our modest-resolution experiments, we prefer to use vertical IEs in making Rydberg assignments.

5.1. CCl_4

Approximate values for the quantum defects of *ns*, *np* and *nd* Rydberg orbitals centred on a C (Cl) atom are predicted to be $\delta = 0.98$ (2.01), 0.58 (1.57) and 0.01 (0.09) [52], respectively. By using vertical IEs for the $(1t_1)^{-1}$, $(3t_2)^{-1}$ and $(1e)^{-1}$ molecular orbitals of CCl_4 of 11.64, 12.51 and 13.37 eV [24], respectively, we can assign the transitions to the six Rydberg states of CCl_4 between 9 and 12 eV as shown in Table 4. The derived quantum defects have values which are sensible for Rydberg orbitals centred on the Cl atoms. This is to be expected since the $1t_1$, $3t_2$ and $1e$ molecular orbitals of CCl_4 are essentially Cl $3p\pi$ non-bonding orbitals which do not involve the central carbon atom [53]. Our assignments agree with those of both the VUV absorption study of Causley and Russell [7] and the fluorescence excitation study of Ibuki et al. [8].

Next, we consider whether the induced fluorescence from photodissociation of these Rydberg states of CCl_4 is due to CCl_2 or to CCl_3. The origin of the CCl_2 $\tilde{A}$–$\tilde{X}$ band occurs at 579 nm [38, 54]. As the peak in the dispersed spectrum (ca. 460–500 nm) occurs at a much lower wavelength, we conclude that the $\tilde{A}^1B_1$ state of CCl_2 is produced vibrationally hot. This phenomenon is not surprising, given the large change in bond angle between the CCl_4 Rydberg state (109° if the state has tetrahedral geometry) and the $\tilde{A}^1B_1$ state of CCl_2 (131° [38]). Combined with the large change in bond angle between the $\tilde{A}^1B_1$ and $\tilde{X}^1A_1$ states of CCl_2 ($\Delta\theta = 22°$ [38]), these two factors will shift the maximum in the $\tilde{A}$–$\tilde{X}$ Franck–Condon envelope to a wavelength much less than $\lambda_{0,0}$. We believe that there is no serious evidence that this emission is due to CCl_3. Breitbarth and Berg [44] were concerned that the peak in CCl_2 $\tilde{A}$–$\tilde{X}$ produced by photodissociation of CCl_4^* occurred at a much lower wavelength than the electronic origin of 579 nm. However, a similar effect has been observed by us for PF_2 $\tilde{B}^2B_2$–$\tilde{X}^2B_1$ emission produced by VUV photodissociation of PF_3 [6], and is a consequence of the method of production of the fragment species in an experiment where vibrational relaxation does not occur. Although ab initio calculations of the valence states of CCl_3 by Hudgens et al. [37] predict excited states with C_{3v} geometry around 25 000 cm^{-1} (i.e., 400 nm) above the ground state, there seems little *direct* evidence that the emission we observe peaking at ca. 460–500 nm is not due to CCl_2. The lifetime of this state measured by Ibuki et al. [8] is also compatible with values obtained for CCl_2 $\tilde{A}^1B_1$ by other methods, such as laser-induced fluorescence spectroscopy [45].

Finally, we consider the lifetime measurement and method of production of the $A^2\Delta$ state of CCl. The lifetime of the $v = 0$ level of this state has been measured by several groups to be ca. 105–110 ns [10, 49, 55], the most complete study for this vibrational level being by Gottscho et al. [55] which showed no rotational level dependence of the lifetime. A study of the dependence of τ on the vibrational level by Larsson et al. [49], however, showed that the lifetime of $v = 1$ dropped to 17–35 ns, the value dependent on which spin–orbit component of $A^2\Delta$ is measured, before increasing again to 86 ns for $v = 2$. The anomalous low value for $v = 1$ is caused by predissociation of the $A^2\Delta$ state by a crossing $^2\Pi$ repulsive state which correlates to ground-state C + Cl products, and only these three lowest vibrational levels of the $A^2\Delta$ state are predicted to be bound [49]. Our value of 53 ± 2 ns (Table 7) is therefore compatible with these other measurements, since our experiment is neither selective in the production of individual vibrational levels of CCl $A^2\Delta$ nor has enough resolution in the secondary monochromator to differentiate emission from different vibrational levels of this state. We should note that a difference in τ_1 and τ_2 by a factor of only ca. three to five is not large enough for the time-resolved decay to fit satisfactorily to a double-exponential function with the correct values of τ_1 and τ_2. The decay will always fit best to a single exponential with an ''average'' value, as is observed here. Our experiment gives no information on whether the other product of the photodissociation is Cl_2 + Cl or 3Cl. Both channels are energetically open at an excitation energy of 16.1 eV. However, the experimental threshold for production of CCl $A^2\Delta$, 14.2 ± 0.1 eV (Fig. 1(c)), lies very close to the thermochemical threshold of CCl $A^2\Delta$ + 3Cl of 14.32 eV (Table 1). A similar effect has been observed for PF $A^3\Pi$ production from PF_3 [6], SiF_2 $\tilde{a}^3B_1$ and $\tilde{A}^1B_1$ production from SiF_4 [5], and B* production from BCl_3 and BBr_3 [2, 3]. In all cases, the experimental threshold lies close to the thermochemical energy for production of the fluorescing fragment with the other halogen atoms formed as isolated

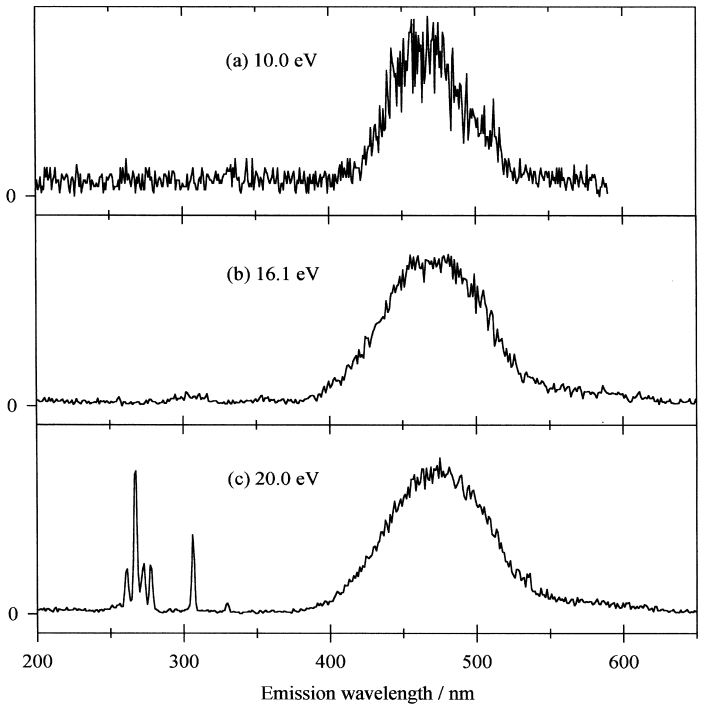

Fig. 8. Dispersed emission spectra recorded at the Bessy 1 synchrotron source for $GeCl_4$ photoexcited at (a) 10.0, (b) 16.1, and (c) 20.0 eV. A LiF window was used in front of the exit slit of the primary monochromator in (a) to suppress second-order radiation at 20.0 eV. A Jobin Yvon H20UV was used as the secondary monochromator with a resolution of 4 nm. No attempt has been made to correct for the sensitivity of the secondary monochromator as a function of wavelength.

atoms. This strongly suggests that, in CCl_4, photodissociation occurs sequentially in multiple steps via excited states of CCl_3 and CCl_2, i.e., $CCl_4^* \rightarrow CCl_3^* + Cl \rightarrow CCl_2^* + Cl + Cl \rightarrow CCl\ A^2\Delta(v) + 3Cl$. A similar mechanism was deduced for PF* and SiF_2^* production from PF_3 and SiF_4 [6, 5].

5.2. $SiCl_4$

Approximate values of quantum defects for *ns*, *np* and *nd* Rydberg orbitals centred on a Si (Cl) atom are predicted to be 1.80 (2.01), 1.36 (1.57) and 0.10 (0.09) [52], respectively. By using vertical IEs for the five outer-valence molecular orbitals of $SiCl_4$ from threshold photoelectron spectroscopy [19], we can assign the symmetries of the six Rydberg states of $SiCl_4$ between 11 and 14 eV which photodissociate to fluorescing states of $SiCl_2$ (Table 5). Since the predicted quantum defects of Si- and Cl-based Rydberg orbitals are very similar, it is difficult to say whether these orbitals are centred on one or the other atom. The derived quantum defects for electron excitation from the $1e$ and $3t_2$ molecular orbitals, however, have values compatible with Rydberg orbitals centred on a Cl atom, as expected since these molecular orbitals are Cl $3p\pi$ non bonding in character. Similarly, the derived quantum defects for electron excitation from the $2t_2$ and $2a_1$ orbitals should be characteristic of both Si and Cl atoms since these orbitals are Si–Cl σ-bonding in character [53]. Our assignments are slightly different from those of Ibuki et al. [18], who use *adiabatic* IEs to determine term values and hence quantum defects.

Unlike CCl_4, the assignment of the fluorescence bands caused by photodissociation of these Rydberg states seems unambiguous. The $\tilde{a}^3B_1$–$\tilde{X}^1A_1$ [40, 29] and $\tilde{A}^1B_1$–$\tilde{X}^1A_1$ [28] bands of $SiCl_2$ have been studied at vibrational and partial-rotational resolution, respectively, and the lifetimes of the $\tilde{a}^3B_1$ and $\tilde{A}^1B_1$ states determined to be 355 ± 8 and 73 ± 2 ns [18]. We

have confirmed the value of the $\tilde{A}$-state lifetime, but the value for the $\tilde{a}^3B_1$ state is too long to measure in a single-bunch experiment. We comment that 355 ns seems very short for the lifetime of the upper state of the spin-forbidden $\tilde{a}$–$\tilde{X}$ transition. This value may not be the true radiative lifetime, but may contain a contribution from rapid intersystem crossing to high vibrational levels of the ground state of $SiCl_2$. Another possibility is that the $\tilde{a}^3B_1$ state is not a pure triplet state, but contains substantial singlet character through spin–orbit coupling with higher-lying singlet states. Both mechanisms have been invoked to explain the short lifetime and the detailed rotational structure of the upper state in the $\tilde{a}^3B_1$–$\tilde{X}^1A_1$ transition in SiF_2 [5, 56]. As with CCl production from CCl_4, our experiment gives no information on whether the other products of the VUV photodissociation of $SiCl_4$ to form $SiCl_2$ ($\tilde{a}^3B_1$ or $\tilde{A}^1B_1$) are Cl_2 or 2Cl. It should be noted that direct dissociation of the $(1e)^{-1}4p$ Rydberg state to form $SiCl_2$ $\tilde{a}^3B_1$ + Cl_2 $X^1\Sigma_g^+$ is formally spin-forbidden, although if the $\tilde{a}^3B_1$ state acquires some singlet character through spin–orbit mixing this selection rule is relaxed. Direct dissociation to form the triplet state of $SiCl_2$ would need Cl_2 to form in an excited triplet state. Conversely, if photodissociation occurs sequentially in two steps ($SiCl_4^* \rightarrow SiCl_3^* + Cl \rightarrow SiCl_2\ \tilde{a}^3B_1 + Cl + Cl$) via an excited state of $SiCl_3$ with doublet symmetry, production of the triplet state of $SiCl_2$ becomes spin-allowed. Photodissociation to the $\tilde{A}^1B_1$ singlet state of $SiCl_2$ is spin-allowed both for a one-step direct dissociation forming Cl_2 and for a two-step sequential dissociation forming 2Cl. What seems quite clear, however, both from our work (clearly shown in the 320 nm action spectrum, Fig. 5(b)) and that of Ibuki et al. [18] is that production of the singlet and triplet B_1 states of $SiCl_2$ is related to photodissociation of specific Rydberg states of $SiCl_4$, and is not related to thermodynamic thresholds. The thresholds to form the $\tilde{a}^3B_1$ and $\tilde{A}^1B_1$ states of $SiCl_2$ (7.4 and 8.8 eV, Table 2) are much lower than the experimental thresholds of 10.0 [18] and 11.8 eV (Fig. 5(b)), respectively.

Emission from the $\tilde{C}^2T_2$ state of $SiCl_4^+$ (adiabatic IE = 15.0 eV) has been observed before in electron-impact ionisation [14], VUV fluorescence excitation [14, 15] and fluorescence coincidence experiments [19], and the results presented in this paper, whilst confirming data obtained elsewhere, yield no new information on the spectroscopy and dynamic properties of this state. At higher photon energies emission due to the Si atom has not been observed before, and is only detected here because of the facility to disperse the fluorescence in the Bessy experiment. The experimental threshold for forming Si* (^3P), 21.8 ± 0.2 eV, corresponds reasonably well to the thermodynamic energy of the excited state of the fluorescing atom formed in conjunction with four isolated halogen atoms. This phenomenon has been observed before for B* formation from both BCl_3 and BBr_3 [2, 3], as well as for CCl* production from CCl_4 (Section 5.1). It strongly suggests that these species are formed by a multi-step sequential mechanism; e.g., $SiCl_4^* \rightarrow SiCl_3^*$ $Cl \rightarrow SiCl_2^* + 2Cl \rightarrow SiCl^* + 3Cl \rightarrow Si^* + 4Cl$. It is very surprising that the lifetimes of the Si* emissions at 254 and 289 nm show bi-exponential (τ_1 = 4–5, τ_2 = 48–49 ns), whereas the emission at 221 nm shows single-exponential (τ = 24.3 ns) behaviour. The only simple mechanism whereby double-exponential behaviour should be observed in an experiment in which the emission wavelength (λ_2) is defined is when two different emitting species are being detected by the secondary monochromator. It is difficult to see what the other species, apart from Si*, could be for λ_2 = 254 and 289 nm. We note, however, that bi-exponential decay is observed for the analogous transitions in Ge* with fairly similar values of τ_1 and τ_2. Although the shorter decay is dominant (Table 7), the long lifetime ''tail'' is unambiguously present in all of these four time-resolved spectra. At present, we cannot explain these results.

5.3. $GeCl_4$

Approximate values for quantum defects of *ns*, *np* and *nd* Rydberg orbitals centred on Ge (Cl) atoms are predicted to be 2.81 (2.01), 2.34 (1.57) and 1.05 (0.09) [52]. Using vertical IEs of the three highest-occupied outer-valence molecular orbitals of $GeCl_4$ from threshold photoelectron spectroscopy of 12.1, 12.67 and 13.1 eV [19], we can assign symmetries to the six Rydberg states of $GeCl_4$ between 9 and 12 eV which photodissociate to fluorescing states of $GeCl_2$. Since the predicted quantum defects of Ge- and Cl-based Rydberg orbitals are rather different, it is now possible to say whether these orbitals are centred on one or the other atom. The transitions from the ground state of

$GeCl_4$ are assigned to *ns* and *np* Rydberg orbitals following electron excitation from one of the $1t_1$, $3t_2$ or $1e$ molecular orbitals (Table 6). The values of the derived quantum defects (*ns* 2.1, *np* 1.6–1.8) are compatible with Cl-based Rydberg orbitals. This is expected since these three molecular orbitals are Cl $3p\pi$ non-bonding in character, with no contribution from the Ge atom. Once again, our assignments are slightly different from those of Ibuki and Kamamoto [20] because they use adiabatic IEs to determine term values and quantum defects of the Rydberg states.

As explained earlier, we assume that the $GeCl_3$ radical plays no direct part in the fluorescence excitation spectra. There has been some controversy over the symmetries of excited states of the $GeCl_2$ molecule (Section 4.3). Following Karolczak et al.'s [30] pioneering high resolution work on the 327 and 448 nm bands, there now seems to be agreement that the former band is due to $\tilde{A}^1B_1$–$\tilde{X}^1A_1$, the latter to $\tilde{a}^3B_1$–$\tilde{X}^1A_1$. Higher valence states of $GeCl_2$ are not known, and the only major unresolved problem is the (non)assignment of the weak emission (band origin 572 nm) first reported by Pathak and Palmer [57] with vibrational parameters for ν_1 and ν_2 identical to those obtained by Karolczak et al. [30] for the ground state of $GeCl_2$. The lifetime of the 327 nm band was measured by Ibuki to be 90 ± 7 ns, that of the 450 nm band 17.4 ± 0.6 μs [39]. Our lifetime data are very limited, mainly because of the narrow range of lifetimes that can be measured. However, our data, that the lifetime of the $\tilde{A}^1B_1$ state is ca. 100–500 ns and that of the $\tilde{a}^3B_1$ state is much longer, do seem to confirm Ibuki's results. There is some ambiguity between the Daresbury fluorescence excitation spectra recorded with different optical filters (Fig. 7) and the Bessy dispersed spectra (Fig. 8). The Daresbury spectra imply that fluorescence from $GeCl_4^*$ Rydberg states between 10 and 12 eV occurs over a wide range of the UV and visible, suggesting that photodissociation to both $\tilde{A}^1B_1$ and $\tilde{a}^3B_1$ states of $GeCl_2$ is happening, whereas the dispersed spectrum at 10 eV (Fig. 8(a)) suggests that the channel to $\tilde{A}^1B_1$ is very minor. Note that *absolute* values of product quantum yields are not obtained in these experiments. We conclude that the channel to $GeCl_2$ $\tilde{a}^3B_1$ followed by $\tilde{a}$–$\tilde{X}$ phosphorescence is the dominant photodissociation pathway for the $GeCl_4^*$ Rydberg states between 9 and 12 eV, and there is some evidence that this is the *only* decay pathway for the lowest Rydberg state at 9.59 eV. To satisfy the spin selection rule (Section 5.2), we suggest that $GeCl_2$ $\tilde{a}^3B_1$ is formed in a two-step sequential process via an excited state of $GeCl_3$ of doublet symmetry; i.e., $GeCl_4^* \rightarrow GeCl_3^*$ Cl $(^2P) \rightarrow GeCl_2$ $\tilde{a}^3B_1$ + Cl (^2P) + Cl (^2P). As with $SiCl_4$, we reiterate that the production of the triplet state of $GeCl_2$ relates to photodissociation of specific Rydberg states of $GeCl_4$, and is not related to thermodynamic thresholds.

Emission from the $\tilde{C}^2T_2$ state of $GeCl_4^+$ (adiabatic IE = 14.6 eV) has been observed before in electron-impact ionisation [14] and VUV fluorescence excitation [14, 15] experiments. As with this state of $SiCl_4^+$, the results reported here, whilst confirming data from these other studies, yield no new information on the spectroscopy or decay dynamics of this state. All the comments made in Section 5.2 on fluorescence from excited states of the Si atom are pertinent to the emission observed at $\lambda < 350$ nm from Ge*. It is important to note that the experimental thresholds for forming Ge* emitting at 267 and 307 nm, 19.0 ± 0.2 and 19.4 ± 0.2 eV, agree within ca. 0.2 eV with the thermochemical thresholds for forming these two excited states with four Cl atoms of 18.8 and 19.1 eV. This is an additional piece of data to support the theory that the excited atom is formed by a multi-step sequential dissociation of $GeCl_4^*$ at these high VUV energies.

6. Conclusions

Using monochromatised synchrotron radiation, we have made a complete study of the processes which lead to fluorescence following VUV photoexcitation of CCl_4, $SiCl_4$ and $GeCl_4$ in the range 9–25 eV. In particular, we have shown that dispersed emission and action spectroscopy are powerful techniques to determine the nature of the emitters when these molecules are photoexcited into their Rydberg states and ionisation continua. This detail of spectroscopic information is not possible to obtain with non-dispersed fluorescence experiments where, using optical filters, only limited information on where the emissions are occurring and hence what the emitters are can be obtained. Furthermore, the ability to disperse the induced fluorescence in the Bessy experiments has

meant that the lifetimes of the different emitters, provided they fall in the range ca. 3–100 ns, can unambiguously be measured.

We have confirmed the results from our earlier study [14, 15] that the $\tilde{C}^2T_2$ state of $SiCl_4^+$ and $GeCl_4^+$ decay radiatively with lifetimes of 38 and 65 ns, respectively, whereas this state of CCl_4^+ does not fluoresce. We have now extended this work to lower photon energies below their ground-state ionisation energy, and have found again that, whereas $SiCl_4$ and $GeCl_4$ behave similarly, CCl_4 behaves in a different manner. Low-lying Rydberg states of CCl_4 photodissociate to the $\tilde{A}^1B_1$ state of CCl_2, whereas these states in $SiCl_4$ and $GeCl_4$ dissociate to both the $\tilde{a}^3B_1$ and $\tilde{A}^1B_1$ states of $SiCl_2$ and $GeCl_2$. The channel to triplet-state production in $GeCl_2$ seems to be dominant. We note, however, that no information on photodissociation of CCl_4^* to the $\tilde{a}^3B_1$ state of CCl_2 is available because the spin-forbidden $\tilde{a}$–$\tilde{X}$ transition in CCl_2, despite being calculated [41], has not been observed. As commented earlier, these experiments give no information on the relative branching ratios to these excited B_1 states of the dichlorides, or on whether photodissociation to these states is a dominant or minor channel compared with photodissociation to the ground state. The action spectrum for $SiCl_4$ leading to $SiCl_2$ $\tilde{A}^1B_1$ production (Fig. 5(b)) confirms that it is photodissociation of specific Rydberg states of $SiCl_4$ that leads to production of this singlet state of $SiCl_2$, and the production of this fragment is not related to thermochemical thresholds. We presume that the same is true for photodissociation of the analogous low-lying Rydberg states of CCl_4 and $GeCl_4$; i.e.,

$$MCl_4 + h\nu_1 \rightarrow MCl_4^* \rightarrow MCl_2^* \ (\tilde{a}^3B_1 \text{ or } \tilde{A}^1B_1) + Cl_2 \text{ or } 2Cl$$

$$MCl_2^* \rightarrow MCl_2 + h\nu_2 \qquad (5)$$

The major unknown is whether photodissociation of MCl_4^* to MCl_2^* occurs as a one-step direct process producing Cl_2 as the other product, or as a two-step sequential process via an excited state of MCl_3 of doublet spin symmetry producing 2Cl as the other products. If the spin selection rules are strictly obeyed and assuming Cl_2 forms in its ground electronic state, photodissociation to $\tilde{A}^1B_1$ can occur by either route, whereas that to $\tilde{a}^3B_1$ must occur via the two-step sequential mechanism.

The simplest photodissociation channel for low-lying Rydberg states of MCl_4 is cleavage of one M–Cl bond to form the MCl_3 free radical. Unlike CF_4 and SiF_4 where photodissociation of such states does lead to fluorescence in the CF_3 and SiF_3 radicals [4, 5], fluorescence from excited states of CCl_3, $SiCl_3$ and $GeCl_3$ has not been observed in these experiments. This could arise for one or more of several reasons. Firstly, photodissociation by M–Cl bond cleavage is a very minor channel. Secondly, photodissociation only produces the ground state of MCl_3. Thirdly, there are no excited states of MCl_3 that fluoresce in the range of the UV/visible that our experiments can detect (190–650 nm).

At higher photon energies different decay channels are observed. For CCl_4, the $A^2\Delta$ state of CCl is produced in the range 14–18 eV with a threshold at the thermochemical energy for producing this fluorescing state of the CCl diatomic with three Cl atoms. For $SiCl_4$ and $GeCl_4$, above the energy of the $\tilde{C}^2T_2$ ionic state from which fluorescence is observed in a non-resonant process, excited states of Si and Ge are formed in the range 19–25 eV. (Note that this fact would be almost impossible to discern from the undispersed fluorescence excitation experiments.) Once again, the theshold for forming these emitting states of Si* or Ge* corresponds to the thermochemical energy to form the appropriate excited atom in conjunction with four Cl atoms. This suggests that at these higher energies the mechanism for production of these more fragmented species involves a sequential, multi-step process; i.e.,

$$MCl_4 + h\nu_1 \rightarrow MCl_4^* \rightarrow MCl_3^* + Cl \rightarrow MCl_2^* + 2Cl \rightarrow MCl^* + 3Cl \rightarrow M^* + 4Cl$$

$$M^* \rightarrow M + h\nu_2 \qquad (6)$$

This mechanism is similar to that invoked to explain B* emission following VUV excitation of BCl_3 and BBr_3 [2, 3], and a similar effect has been observed for P^* emission from PCl_3 and PBr_3 [58]. We note that atomic emission has never been observed from the central atom for the fluorides of Groups III, IV and V (i.e., BF_3, CF_4, SiF_4, PF_3). This may simply be a

matter of energetics, that dissociation to M* + *n*F lies at a higher energy on account of the stronger M–F bonds, and falls outside the range of the primary monochromator (7–25 eV) used in these experiments. It is difficult to explain otherwise why this phenomenon should only be associated with the chlorides and bromides of these Group III–V halide molecules.

Acknowledgements

We thank EPSRC and the Daresbury Laboratory for a Research Grant, a Post-Doctoral Fellowship (D.M.S.), Research Studentships (K.J.B., D.P.S.) and a CASE award (K.J.B.). H.B. thanks the Deutsche Forschungsgemeinschaft for a Post-Doctoral Fellowship. The EU Training and Mobility of Researchers programme (contract number ERBFMGE-CT-950031) and the British Council (ARC bilateral programme with Germany, contract number 707) are also acknowledged for funding of the Bessy project. Finally, we thank Dr M.A. Hayes of the Daresbury Laboratory for programming and advice with the use of the lifetime fitting programme FLUOR.

References

[1] R.P. Tuckett, Chem. Soc. Rev. 19 (1990) 439.
[2] H. Biehl, J.C. Creasey, D.M. Smith, R.P. Tuckett, K.R. Yoxall, H. Baumgärtel, H.W. Jochims, U. Rokland, J. Chem. Soc., Faraday Trans. 91 (1995) 3073.
[3] H. Biehl, D.M. Smith, R.P. Tuckett, K.R. Yoxall, H. Baumgärtel, H.W. Jochims, U. Rokland, Mol. Phys. 87 (1996) 1199.
[4] H. Biehl, K.J. Boyle, R.P. Tuckett, H. Baumgärtel, H.W. Jochims, Chem. Phys. 214 (1997) 367.
[5] H. Biehl, K.J. Boyle, D.P. Seccombe, D.M. Smith, R.P. Tuckett, K.R. Yoxall, H. Baumgärtel, H.W. Jochims, J. Chem. Phys. 107 (1997) 720.
[6] H. Biehl, K.J. Boyle, D.P. Seccombe, R.P. Tuckett, H. Baumgärtel, H.W. Jochims, J. Chem. Phys. 108 (1998) 857.
[7] G.C. Causley, B.R. Russell, J. Elect. Spectrosc. Relat. Phenom. 11 (1977) 383.
[8] T. Ibuki, N. Takahashi, A. Hiraya, K. Shobatake, J. Chem. Phys. 85 (1986) 5717.
[9] L.C. Lee, M. Suto, Chem. Phys. 114 (1987) 423.
[10] I. Tokue, T. Honda, Y. Ito, Chem. Phys. 140 (1990) 157.
[11] M. Kusakabe, Y. Ito, I. Tokue, Chem. Phys. 170 (1993) 243.
[12] J.J. Tiee, F.B. Wampler, W.W. Rice, J. Chem. Phys. 72 (1980) 2925.
[13] M. Tsuji, M. Furasawa, T. Mizuguchi, T. Muraoka, J. Chem. Phys. 97 (1992) 245.
[14] I.R. Lambert, S.M. Mason, R.P. Tuckett, A. Hopkirk, J. Chem. Phys. 89 (1988) 2675.
[15] I.R. Lambert, S.M. Mason, R.P. Tuckett, A. Hopkirk, J. Chem. Phys. 89 (1988) 2683.
[16] T. Ibuki, N. Washida, U. Itoh, Y. Toyoshima, H. Onuki, Chem. Phys. Lett. 136 (1987) 447.
[17] K. Kameta, M. Ukai, T. Numazawa, N. Terazawa, Y. Chikahiro, N. Kouchi, Y. Hatano, K. Tanake, J. Chem. Phys. 99 (1993) 2487.
[18] T. Ibuki, M. Kono, Y. Asari, A. Hiraya, K. Shobatake, J. Chem. Phys. 106 (1997) 4853.
[19] D.M. Smith, R.P. Tuckett, K.R. Yoxall, K. Codling, P.A. Hatherly, J.F.M. Aarts, M. Stankiewicz, J. Chem. Phys. 101 (1994) 10559.
[20] T. Ibuki, A. Kamamoto, Chem. Phys. Lett. 260 (1996) 314.
[21] K.J. Boyle, Ph.D. thesis, University of Birmingham, 1998.
[22] G.K. Jarvis, Ph.D. thesis, University of Birmingham, 1997.
[23] C.M. Gregory, M.A. Hayes, G.R. Jones, E. Pantos, Technical Memorandum, Daresbury Laboratory, ref. DL/SCI/TM98E, 1994.
[24] P.J. Bassett, D.R. Lloyd, J. Chem. Soc. A (1971) 641.
[25] J.C. Creasey, I.R. Lambert, R.P. Tuckett, K. Codling, L.J. Frasinski, P.A. Hatherly, M. Stankiewicz, D.M.P. Holland, J. Chem. Phys. 93 (1990) 3295.
[26] J. Tellinghuisen, D.K. Chakraborty, Chem. Phys. Lett. 134 (1987) 565.
[27] N. Washida, M. Suto, S. Nagase, U. Nagashima, K. Morokuma, J. Chem. Phys. 78 (1983) 1025.
[28] J. Karolczak, D.J. Clouthier, Chem. Phys. Lett. 201 (1993) 409.
[29] K. Du, X. Chen, D.W. Setser, Chem. Phys. Lett. 181 (1991) 344.
[30] J. Karolczak, Q. Zhuo, D.J. Clouthier, W.M. Davis, J.D. Goddard, J. Chem. Phys. 98 (1993) 60.
[31] M.W. Chase, C.A. Davies, J.R. Downey, D.J. Frurip, R.A. MacDonald, A.N. Syverud, J. Phys. Chem. Ref. Data 14 (1985).
[32] J.W. Hudgens, R.D. Johnson, R.S. Timonen, J.A. Seetula, D. Gutman, J. Phys. Chem. 95 (1991) 4400.
[33] J. Tamas, G. Czira, A.K. Maltsev, O.M. Nefedov, J. Organometallic Chem. 40 (1972) 311.
[34] O. Uy Manuel, D.W. Muenow, J.L. Margrave, Trans. Faraday Soc. 65 (1969) 1296.
[35] F. Danis, F. Caralp, B. Veyret, H. Loirat, R. Lesclaux, Int. J. Chem. Kinetics 21 (1988) 715.
[36] T. Ellermann, Chem. Phys. Letts. 189 (1992) 175.
[37] J.W. Hudgens, R.D. Johnson, B.P. Tsai, S.A. Kafafi, J. Am. Chem. Soc. 112 (1990) 5763.
[38] D.J. Clouthier, J. Karolczak, J. Chem. Phys. 94 (1991) 1.
[39] T. Ibuki, Chem. Phys. Lett. 169 (1990) 64.
[40] H. Sekiya, Y. Nishimura, M. Tsuji, Chem. Phys. Lett. 176 (1991) 477.
[41] E.A. Carter, W.A. Goddard, J. Phys. Chem. 90 (1986) 998; ibid. 91 (1987) 4651.
[42] R.D. Verma, R.S. Mulliken, J. Mol. Spectrosc. 6 (1961) 419.
[43] C.E. Moore, Atomic Energy Levels (1971), NBS Circular NSRDS-NBS 35, vols. 1 and 2.

[44] F.W. Breitbarth, D. Berg, Chem. Phys. Lett. 149 (1988) 334.
[45] R.E. Huie, N.J.T. Long, B.A. Thrush, Chem. Phys. Lett. 51 (1977) 197.
[46] V.E. Bondybey, J. Mol. Spectrosc. 64 (1977) 180.
[47] J. Moc, Z. Latajka, H. Ratajczak, Chem. Phys. Lett. 136 (1987) 122.
[48] M. Suzuki, N. Washida, G. Inoue, Chem. Phys. Lett. 131 (1986) 24.
[49] M. Larsson, M.R.A. Blomberg, P.E.M. Siegbahn, Mol. Phys. 46 (1982) 365.
[50] J.C. Green, M.L.H. Green, P.J. Joachim, A.F. Orchard, D.W. Turner, Phil. Trans. Roy. Soc. Lond. A 268 (1970) 111.
[51] R.L. Asher, E.H. Appleman, B. Ruscic, J. Chem. Phys. 105 (1996) 9781.
[52] C.E. Theodosiou, M. Inokuti, S.T. Manson, Atomic Data and Nuclear Data Tables 35 (1986) 473.
[53] R.N. Dixon, R.P. Tuckett, Chem. Phys. Lett. 140 (1987) 553.
[54] R. Kiefer, A. Siegel, A. Schultz, Chem. Phys. Lett. 59 (1978) 298.
[55] R.A. Gottscho, R.H. Burton, G.P. Davis, J. Chem. Phys. 77 (1982) 5298.
[56] J. Karolczak, R.H. Judge, D.J. Clouthier, J. Am. Chem. Soc. 117 (1995) 9523.
[57] C.M. Pathak, H.B. Palmer, J. Mol. Spectrosc. 31 (1969) 170.
[58] K.J. Boyle, G.K. Jarvis, R.P. Tuckett, J. Chem. Soc., Faraday Trans. 94 (1998) 2073.